

<https://doi.org/10.1038/s42003-025-07451-y>

Dietary caloric input and tumor growth accelerate senescence and modulate liver and adipose tissue crosstalk

Check for updates

José Xavier do Nascimento Júnior^{1,2}, Júlia da Conceição Gomes^{1,2}, Ricardo Imbroisi Filho¹, Helber de Maia Valença¹, Jéssica Ristow Branco¹, Amanda Bandeira Araújo¹, Amanda de Oliveira Esteves Moreira¹, Letícia Diniz Crepaldi¹, Larissa Pereira Paixão¹, Alan C. Ochioni¹, Thainá M. Demaria¹, João Gabriel Bernardo Leandro¹, Livia Marques Casanova¹, Mauro Sola-Penna¹ & Patricia Zancan¹ ✉

Metabolic alterations are related to tumorigenesis and other age-related diseases that are accelerated by “Westernized” diets. In fact, hypercaloric nutrition is associated with an increased incidence of cancers and faster aging. Conversely, lifespan-extending strategies, such as caloric restriction, impose beneficial effects on both processes. Here, we investigated the metabolic consequences of hypercaloric-induced aging on tumor growth in female mice. Our findings indicate that a high-fat high-sucrose diet increases tumor growth mainly due to the boosted oxidation of glucose and fatty acids. Consequently, through an increased expression of lactate, IGFBP3, and PTHLH, tumors modulate liver and white adipose tissue metabolism. In the liver, the induced tumor increases fibrosis and accelerates the senescence process, despite the lower systemic pro-inflammatory state. Importantly, the induced tumor induces the wasting and browning of white adipose tissue, thereby reversing diet-induced insulin resistance. Finally, we suggest that tumor growth alters liver-adipose tissue crosstalk that upregulates *Fgf21*, induces senescence, and negatively modulates lipids and carbohydrates metabolism even in caloric-restricted-fed mice.

Epidemiological studies have revealed an association between obesity and an increased incidence and progression of cancer^{1,2}. In fact, obesity is the second most preventable cause of cancer³. Aging and cancer have been described as two different manifestations of the accumulation of cellular damage⁴, which is accelerated by obesity⁵. Thus, there is growing concern regarding the relationship between obesity and cancer due to the increasingly aging population and the current obesity pandemic.

There has been a rapid increase in the interest in therapeutically targeting senescence, which manifests as efforts to improve healthy aging and reduce age-related diseases^{6,7}. However, it is important to indicate that aging and senescence are not synonymous, since cells can undergo senescence, regardless of organismal age^{8,9}. The “westernized” lifestyle, which includes a high-calorie diet and a sedentary lifestyle, can accelerate aging. In contrast, lifespan-extending strategies, such as calorie restriction (CR), can promote metabolic fitness⁴. Both processes, although opposite, take effect through the modulation of signaling pathways that respond to the fluctuations of nutritional levels, such as the insulin and IGF-1 signaling pathways, in

addition to the nutritional sensors AMP-activated protein kinase (AMPK) and sirtuins^{10,11}. Indeed, the PI3K-AKT-mTOR pathway has prominent aging-modulating effects.

We have previously shown that a high-fat high-sucrose (HFHS) diet promotes tumor growth due to an increased response to insulin, in addition to inducing tumor aggressiveness¹². Moreover, an HFHS diet reduced the expression of cellular senescence markers in the tumors¹². However, gene–environment interactions—such as those induced by high-fat diets or CR—molecularly modulate body physiology and play a key role in the pathogenesis of metabolic diseases^{13,14}. Yet, it is not clear how obesity and aging attenuation or acceleration through CR or a high-calorie diet influence tumorigenesis or tumor growth and its consequences on the biology of different body tissues.

Here, we addressed this important question by investigating the metabolic consequences induced by changing the dietary regimen of adult female C57BL/6J mice and their impact on tumor growth. Thus, mice aged 12 weeks were fed for 26 weeks with a Chow, CR, or HFHS diet. In the

¹The MetaboliZSm Group, Departamento de Biotecnologia Farmacêutica, Faculdade de Farmácia, Universidade Federal do Rio de Janeiro, Rio de Janeiro, Brazil.

²These authors contributed equally: José Xavier do Nascimento Júnior, Júlia da Conceição Gomes. ✉e-mail: pzancan@me.com

twenty-third week, an ectopic tumor was induced by a subcutaneous injection of B16F10 cells on the back of the animals. Our data indicate that tumor growth impairs glucose tolerance in Chow-fed mice, while the HFHS diet increases lipids and glucose metabolism in tumors, thereby inducing the expression of energy balance disruptors that act on the liver and adipose tissue of these mice. Therefore, we observed an acceleration of aging in tumor-bearing HFHS-fed animals as well as increased fibrosis in the liver. Tumor growth and the HFHS diet-induced hepatic insulin resistance and impaired lipid metabolism in this tissue despite presenting a lower systemic inflammatory profile. We also observed an alteration in liver-white adipose tissues (WAT) crosstalk and a surprising increase in browning and reversal of insulin resistance in WAT due to tumor growth in mice. Based on these results, we discuss the interrelationship among diet, aging, and tumor growth and their consequences for whole-body physiology and health.

Materials and methods

Cell culture

B16F10, a mouse-derived skin melanoma cell line, was obtained and authenticated by the Cell Bank of Rio de Janeiro (BCRJ; www.bcrj.org.br, Duque de Caxias, RJ, Brazil). The cells were grown and maintained in Dulbecco's Modified Eagle's medium (DMEM) containing 25 mM glucose supplemented with 10% (v/v) heat-inactivated fetal bovine serum (FBS) (Invitrogen, São Paulo, SP, Brazil) at 37 °C in a 5% CO₂ atmosphere¹⁵. HuH-7 hepatoma (a kind gift of Dr. A. Da Poian, UFRJ, Brazil) was grown in monolayer culture in high-glucose DMEM supplemented with 10% (v/v) FBS and 1% (v/v) antibiotic/antimycotic solution in a humidified atmosphere of 10% CO₂ at 37 °C. 3T3-L1 fibroblasts (BCRJ; www.bcrj.org.br, Duque de Caxias, RJ, Brazil) were grown in monolayer culture in high-glucose DMEM supplemented with 10% (v/v) FBS and 1% (v/v) antibiotic/antimycotic solution in a humidified atmosphere of 10% CO₂ at 37 °C. Two days after confluence, 3T3-L1 fibroblasts were differentiated into adipocytes in DMEM containing 10% FBS, 115 µg/ml 3-isobutyl-1-methylxanthine, 390 ng/ml dexamethasone, and 10 µg/ml insulin for 4 days, then the medium was replaced with DMEM supplemented with 10% FBS and 5 µg/ml insulin for an additional 4 days. The medium was then replaced by DMEM containing 10% FBS until >80% of the cells exhibited an adipocyte morphology, typically between 8 days and 12 days after differentiation¹⁶.

Animals and induction of tumor

Adult female C57BL/6J mice (aged 12 weeks) were housed in the animal facility of the Faculty of Pharmacy, Federal University of Rio de Janeiro, Brazil. The animals were kept at a controlled temperature (23 °C) on a 12-h light/dark cycle in controlled humidity¹². The sample size was calculated as previously described in ref. 17. The protocol and all procedures used in this current work have been previously approved by the Animal Care and Use Committee of the Health Sciences Center of the Federal University of Rio de Janeiro (CEUA/CCS/UFRJ 177/18). Mice were put on a sterilized standard rodent diet (4.4% fat by kcal, total 3.6 kcal/g of diet, AIN-93M, Pragsoluções Biotécnicas, Jaú, SP, Brazil) for two weeks to acclimate. At the beginning of the protocol (Week 0), the animals were 12-weeks-old and were randomly divided into 3 groups that were either kept on the standard diet (Chow), transferred to an HFHS diet containing 65.4% fat and 19.6% carbohydrates (sucrose) by kcal, or kept on a CR diet (30% of Chow group) for 26 weeks. The HFHS diet (Pragsoluções Biotécnicas, Jaú, SP, Brazil) was prepared as previously described in ref. 18. Bodyweight gain and food intake were evaluated once and twice a week, respectively. In week 23, B16F10 cells (10,000 cells suspended in 50 µL phosphate-buffered saline) or saline buffer (for the control group) were subcutaneously injected into the back of the mice in all groups, forming a solid tumor with the dimensions ~0.6 ± 0.2 cm³ after 10 days. In week 26, the mice were anesthetized in saturated chambers with isoflurane and sacrificed by cardiac puncture. Fifteen minutes before sacrifice, the mice were injected intraperitoneally with saline (0.9% NaCl) or 2 IU/kg of insulin solution. The tumor, tissues, and organs were collected and weighted and plasma samples were obtained

by centrifugation (3000 × g for 15 min at 4 °C). Additionally, the tumor volume was determined using a caliper according to the procedure described in the literature¹⁹. Liver samples were collected and fixed in 4% buffered formalin. All the materials were identified and snap-frozen in liquid nitrogen. Further, all the samples were included in data analyses.

Oral glucose tolerance test (oGTT)

The oral glucose tolerance test (oGTT) was performed as previously described; moreover, after a 3-h fasting period, glucose tolerance was assessed by the oral administration of 2 g of dextrose per kg of body weight by gavage. Glycemia was assessed from the caudal vein at time 0 (before gavage) and 15 min, 30 min, 60 min, and 120 min after administration using a FreeStyle Precision Neo glucometer (Abbott Laboratories, Chicago, IL, USA)²⁰.

Plasma insulin

Serum insulin quantification was assessed by an enzyme-linked immunosorbent assay (ELISA) using Insulin Mouse ELISA Kit (ThermoFisher, Carlsbad, CA) following the manufacturer's instructions.

Plasma and liver lipids

Liver lipids were extracted using Folch's method²¹ and the quantification of liver and plasma cholesterol and triglycerides were assessed using the commercial kits Cholesterol 250 and Triglyceride Enzymatic (Doles Reagentes, Panamá, GO, Brazil), respectively, according to the manufacturer's recommendation, as previously described in ref. 20.

Hepatic enzymes

Plasma alanine aminotransferase (ALT) and aspartate aminotransferase (AST) were evaluated using commercial kits (Doles Reagentes, Panamá, GO, Brazil) following the manufacturer's protocol, as previously described in ref. 15.

Western blotting

The samples of the powdered tumor, liver, and gonadal white adipose tissue (gWAT) were lysed with RIPA buffer supplemented with a Protease inhibitor cocktail (Sigma-Aldrich, St. Louis, MO, USA). The protein extraction, SDS-PAGE (8–12% acrylamide gels), and PVDF membrane transfer were performed as previously described in ref. 22. The membranes were pre-cut after Ponceau S staining, blocked, and incubated overnight with the primary antibodies, as presented in Table S1. After overnight incubation, the membranes were incubated with the appropriate secondary antibodies, and Western blotting was conducted, as previously described, using a C-DiGit Blot Scanner (LiCor, Lincoln, NE, USA). The quantifications were performed using Image J64 (Rasband, W.S., ImageJ, U.S. National Institutes of Health, Bethesda, Maryland, USA, <https://imagej.nih.gov/ij/>, 1997–2018; NIH, USA)²³.

Enzymatic activities

The enzymatic activities were evaluated after the protein extraction of powdered tumor samples (40 µg) with RIPA buffer supplemented with a Protease inhibitor cocktail (Sigma-Aldrich, St. Louis, MO, USA) as previously described in ref. 24. Briefly, samples were centrifuged at 8000 × g for 15 min, 4 °C, and the supernatant was collected. Protein concentration was assessed according to the manufacturer's description (Pierce BCA Protein Assay Kit, ThermoScientific, USA). Enzymatic kinetics were initiated by adding 10 µL of the cell-free homogenates in appropriate reaction media¹⁵. Hexokinase (HK), phosphofructokinase (PFK), and pyruvate kinase (PK) activities were assessed by NADH oxidation or NAD⁺ reduction determined by measuring the absorbance at 340 nm in a microplate reader (VICTOR 3, PerkinElmer). Lactate dehydrogenase (LDH) activity was assessed in a reaction media containing 50 mM Tris-HCl (pH 7.4), 1 mM MgCl₂, 120 mM KCl, and 5 mM NAD⁺ and 5 mM sodium lactate (to evaluate Lactate > Pyruvate flux) or 5 mM NADH and 5 mM sodium pyruvate (to evaluate Pyruvate > Lactate flux). For the enzymatic analyses,

NADH oxidation or NAD⁺ reduction was determined by measuring the absorbance at 340 nm in a microplate reader (VICTOR 3, PerkinElmer).

B16F10 cell culture supplemented with mouse serum

Mouse serum was obtained by cardiac puncture as previously described. A pool of serum mice from CR, Chow, or HFHS was heat-inactivated, centrifuged, aliquoted, and frozen until utilization in this assay²⁵. B16F10 cells (2×10^5) were seeded in 12-well plates and the treatment was conducted when the cells reached 70% of confluence. Then, the medium was replaced with a fresh DMEM high glucose (25 mM) supplemented with 2% mouse serum of all experimental groups without tumors (CR, Chow, and HFHS) for 48 h. At the end of the experiment, mRNA extraction was performed.

Conditioned medium and cell treatment

B16F10 cells (2×10^5) were seeded in 12-well plates and treatments were conducted when cells reached 70% of confluence. Conditioned medium (CM) was obtained from HuH-7 or 3T3-L1 cells treated with DMEM high glucose (25 mM) supplemented or not with 200 μ M of palmitic acid (PA) for 24 h. After the treatment, cell-cultured media were collected, centrifuged, and utilized for treatment. B16F10 cells were treated with DMEM high glucose (25 mM) supplemented or not with 200 μ M of PA or with the CM obtained from Huh7 and 3T3-L1 for 24 h and subjected to mRNA extraction.

qPCR

B16F10 cells from in vitro experiments or tumor, liver, and gWAT samples were powdered and subjected to mRNA extraction using TRIzol reagent (Thermo Fisher, Carlsbad, CA, USA) following the manufacturer's procedures. For cDNA synthesis, a high-capacity cDNA reverse transcription kit (Thermo Fisher, Carlsbad, CA, USA) was used following the manufacturer's recommended protocol. Further, quantitative analysis of mRNA expression levels was conducted utilizing dye-based GoTaq qPCR Master Mix (Promega, Fitchburg, WI, USA) based on the selection of oligo pairs. The qPCR reactions were performed using the QuantStudio 5 platform (Thermo Fisher, Carlsbad, CA, USA). Detailed protocols for dye-based reactions can be found elsewhere²⁰. The relative mRNA expression levels were determined using the $2^{-\Delta\Delta Ct}$ or $2^{-\Delta Ct}$ method according to the high international standards established²⁶. Further, housekeeping genes were selected as reference genes since their expression did not vary with any of the treatments (data not shown). The optimization of qPCR conditions was performed in accordance with international standards²⁶. Detailed information regarding the primers utilized in this study is presented in Table S2.

Processing and staining of hepatic tissue

Liver samples, after being removed and sectioned, were fixed in a 4% buffered formalin solution at pH 7.2 for subsequent histological analyses. The fragments were dehydrated using increasing concentrations of ethyl alcohol (70%, 80%, 90%, and 100% in two baths of 20 min each). After dehydration, the specimens were cleared in two successive baths of xylene (20 min each), impregnated in two baths of paraffin (20 min each), and finally immersed and embedded in paraffin. All processing was performed with the aid of a semi-closed sectioning tissue processor, model Leica TP1020. Subsequently, histological sections that were 5 μ m thick were obtained using a microtome, model Leica RM2125RT, and collected on slides and placed in an oven at 37 °C for 24 h to dry²⁷.

Hematoxylin and eosin (HE) staining

The slides were deparaffinized in two baths of xylene, hydrated in a series of decreasing concentrations of ethyl alcohol (100%, 90%, and 70%), and washed in distilled water. Staining was performed with Harris hematoxylin for 10 s, followed by washing in running water for 5 min. Subsequently, the sections were stained with eosin for 10 s²⁷. After a quick wash in distilled water, the sections were dehydrated in ethyl alcohol (70%, 90%, and 100%), cleared in two baths of xylene, and mounted with coverslips using Entellan (Entellan® new, Merck).

Picrosirius red staining

To stain and highlight collagen fibers, histological slides were treated with picrosirius solution (3 g of Sirius Red F3BA in 100 ml of saturated aqueous picric acid solution). After a bath in distilled water, the slides were immersed in picrosirius solution for 1 h, followed by a bath in 0.01 N HCl for 2 min²⁸. After a quick wash in distilled water, the sections were dehydrated in ethyl alcohol (70%, 90%, and 100%), cleared in two baths of xylene, and mounted with coverslips using Entellan (Entellan® new, Merck).

Gomori's reticulin

To stain and highlight the reticular fibers, the slides were immersed in 1% potassium permanganate and 3% oxalic acid solutions, washed in running water, and immersed in 2% iron alum solution. After washing, ammoniacal silver nitrate solution was applied to the slides for 1 min, followed by another wash in distilled water for 5 min and immersion in 1% gold chloride solution for 10 min. After this immersion, the slides were washed again in distilled water for 2 min and immersed in 5% sodium thiosulfate for 1 min²⁹. After a quick wash in distilled water, the sections were dehydrated in ethyl alcohol (70%, 90%, and 100%), cleared in two baths of xylene, and mounted with coverslips using Entellan (Entellan® new, Merck).

Microscope analysis

The slides were analyzed under a light microscope (40 \times objective), and 10 fields per slide were captured. The average steatotic area and reticular fibers were evaluated using the Cyclops Histopathological Tool software (UFSC—Federal University of Santa Catarina, BR—<http://chptool.telemedicina.ufsc.br/>).

Metabolomic analysis of animal serum pools

Serum from control and tumor-bearing animals ($n = 4-8$) from all experimental groups (CR, Chow, and HFHS) were pooled and sent for metabolomic analysis at Nemo Metabolômica (LADETEC-IQ/UFRJ). The description of the method and analyses performed is described in S7.

Lipid and metabolite content evaluation in tissues

Lipid content evaluation in tissue was performed by thin-layer chromatography (TLC) as described previously in ref. 30. Briefly, the livers and gWAT were used (50 mg of powdered tissues) to extract lipids using a 250 μ l chloroform/methanol (2:1) mixture. After adding the solvent, tissues were vigorously mixed in a Vortex at maximal speed for 30 s for each sample. Then, the mixtures were centrifuged (6000 \times g, 15 min) and the organic phase was extracted and completely dried overnight in a hood. The dried content was dissolved in pure Hexane and applied in a TLC plate (pre-coated silica gel 60 F plates 20 \times 20 cm, Merck, Germany). TLC was resolved in hexane:diethyl-ether:acetic acid (H:D:A) (70:10:0.1, v/v/v), and lipids were revealed using Iodine (I₂). Revealed TLC was scanned and bands were analyzed using ImageJ software.

The aqueous (methanolic) phases obtained above were dried overnight in a hood and resuspended in 50 μ l distilled water. Glycerol was quantified using a coupled enzyme system, containing glycerol kinase (2 mU/ml) and α -glycerophosphate dehydrogenase (5 mU/ml) in a reaction medium containing 50 mM Tris-HCl (pH 7.4) and 5 mM NAD⁺, which reduction was followed in a microplate reader at 340 nm. Similarly, fructose-1,6-bisphosphate was quantified using aldolase (2 mU/ml), triosephosphate isomerase (4 mU/ml), and α -glycerophosphate dehydrogenase (5 mU/ml) in a reaction medium containing 50 mM Tris-HCl (pH 8.2) and 5 mM NADH, which oxidation was followed in a microplate reader at 340 nm. Acetyl-Coa was evaluated in a coupled system containing citrate synthase (10 mU/ml), aconitase (4 mU/ml), and isocitrate dehydrogenase (2 mU/ml), in a medium containing 50 mM Tris-HCl (pH 7.4), 10 mM oxaloacetate and 5 mM NAD⁺, which reduction was followed in a microplate reader at 340 nm. Lastly, oxaloacetate was evaluated using malate dehydrogenase (10 mU/ml) in a reaction medium containing 50 mM Tris-HCl (pH 8.2) and 5 mM NADH, which oxidation was followed in a microplate

reader at 340 nm. All assays were conducted in a final volume of 150 μ l using 10 μ l of the resuspended material.

Statistical analysis and reproducibility

Prism 10 for Mac (GraphPad Software Inc., La Jolla, CA, USA) was used for graphical and statistical analysis. Student's *t*-test, Mann–Whitney non-parametric test, one-way ANOVA followed by Tukey's post-test, and two-way ANOVA followed by Sidak's post-test were used as appropriate, as previously described in ref. 26. Detailed information regarding the number of experiments and significance levels are presented in the legend of each figure.

Reporting summary

Further information on research design is available in the Nature Portfolio Reporting Summary linked to this article.

Results

In order to investigate the contribution of Western diet-induced aging on tumor growth, we fed young adult female C57BL/6J mice for 26 weeks with an HFHS diet (HFHS group) and compared them with animals that were fed a standard diet (Chow group), both *ad libitum* or subjected to approximately 30% caloric restriction (CR group). At week 23, an ectopic tumor was induced by subcutaneously injecting B16F10 melanoma cells on the back of the animals (Fig. 1A). At the end of the protocol, mice whole-body weight gain and the weight of their tissues and organs, in addition to the tumor growth, were evaluated. Our data reveal that, after 26 weeks of diet, the CR group lost weight, while the HFHS group gained weight as compared to the Chow group (Fig. 1B). Additionally, we also evaluated mice carcass weight after removing the tumors and compared their weight to that of their control counterparts. Only the HFHS group presented a significant variation in the carcass weight after tumor removal (Fig. 1C). This result is a consequence of the impact of the diet on tumor growth since our data reveal that tumors increase in weight (Fig. 1D) and volume (Fig. 1E) in accordance with the caloric intake (i.e., CR < Chow < HFHS). Moreover, we evaluated the weight of the liver (Fig. 1F), inguinal (iWAT, Fig. 1G) and gonadal (gWAT, Fig. 1H) white adipose tissues, gastrocnemius (Fig. S1a) and quadriceps muscles (Fig. S1b), and the heart (Fig. S1c). Among these tissues and organs, only the adipose tissues had reduced weight in tumor-bearing mice, particularly in the HFHS-fed groups (Fig. 1G, H), thereby suggesting that WAT metabolism may be related to tumor growth.

As expected, after 26 weeks on the HFHS diet, mice presented impaired glucose tolerance, as revealed through an oral glucose tolerance test (oGTT) (Fig. 1I, L) and high-fasting glycemia as compared to the CR and Chow groups (Fig. 1K). Chow and CR groups presented similar results for oGTT and fasting glycemia, although the CR group presented lower fasting insulin levels (Fig. 1N), thereby suggesting an improvement in insulin responsiveness as compared to the Chow group. This picture changes in tumor-bearing animals, where an impairment in glucose tolerance was observed in the Chow group (but not in the CR group) (Fig. 1J, M). Indeed, in all tumor-bearing groups, we observed similar levels of fasting glycemia (~7 mM; Fig. 1K, black vs hatched bars). Curiously, fasting glycemia and insulinemia were found to be decreased in the HFHS groups when comparing tumor-bearing with control mice, an effect that was not observed in the CR or Chow groups (Fig. 1K, N). Moreover, insulinemia was also evaluated after intraperitoneal administration of 2 IU/kg insulin, 15 min. before euthanasia, where all the groups presented similar insulin levels, except the HFHS control group that presented higher insulinemia (Fig. S1d, dotted lines indicate fasting insulinemia in tumor-free mice). The impaired glucose tolerance observed in tumor-bearing Chow mice can be partially due to the upregulation of *Pck1* mRNA (coding for PEPCK) in the livers of these animals (Fig. S1e).

Furthermore, we evaluated the serum lipid profile, where we observed an increase in circulating triglycerides (TG) induced by tumor growth in the Chow and HFHS groups as compared to their control counterparts

(Table 1). Nevertheless, a great variation in the lipid profile was observed in the circulating LDL of tumor-bearing HFHS mice, which was more than double as compared to any other group (Table 1). On account of the results described above, we decided to evaluate the tumor's metabolic profile and its consequences for the physiology of liver and adipose tissues.

Tumor metabolism is boosted by the HFHS diet

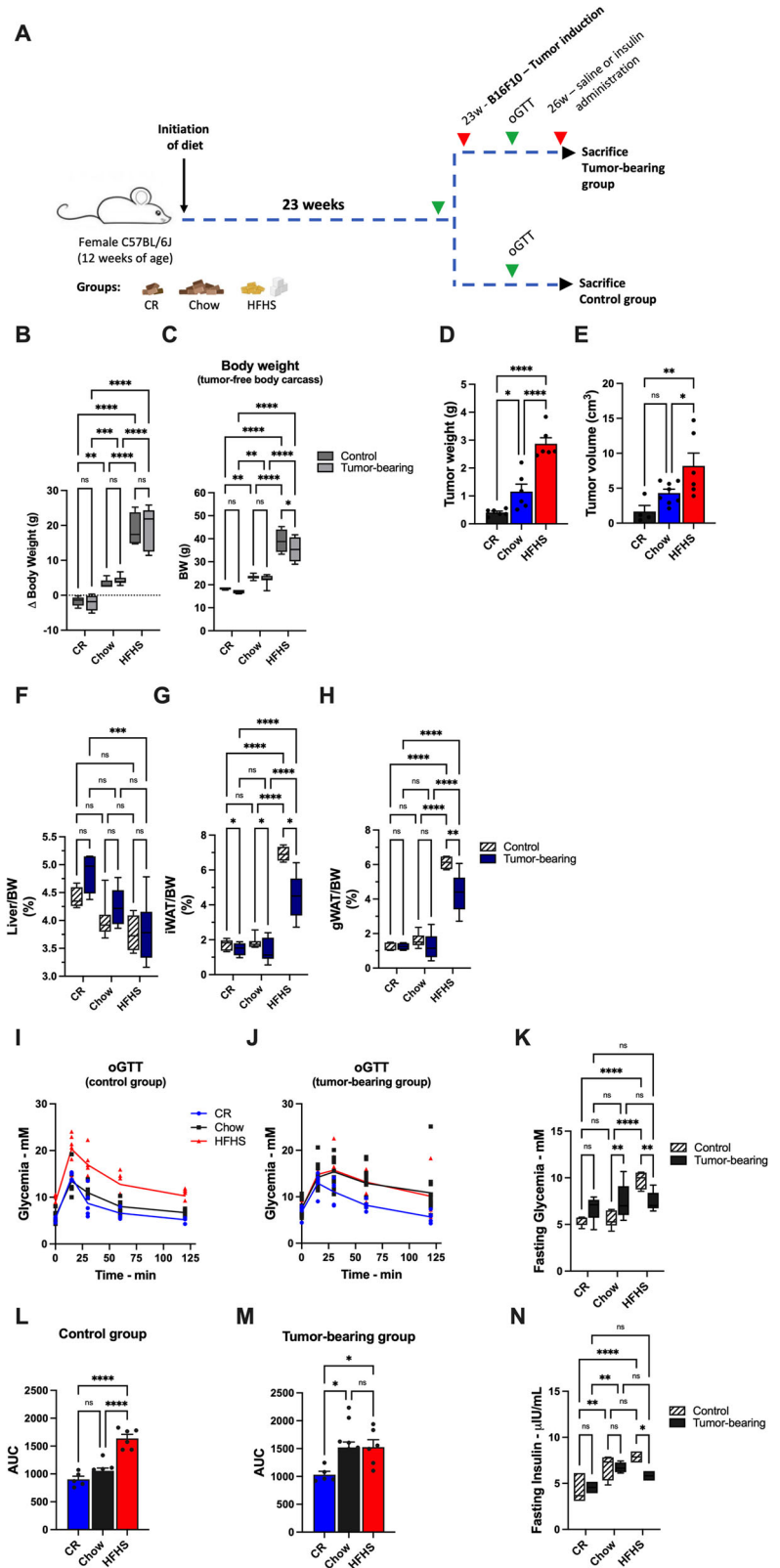
The metabolism of lipids and carbohydrates was assessed in the tumor tissues of mice fed with different dietary regimens, and our data indicated an adaptation of tumor growth in mice fed with the HFHS diet to better metabolize lipids. This statement is supported by the upregulation of different genes related to fatty acid metabolism, such as *Fabp3*, *Cd36*, *Cpt1a*, and *Ppara* (Fig. 2A–D, respectively), thereby suggesting an increased fatty acid uptake, transport, and oxidation. PPAR α is also a regulator of glucose metabolism, which was evidenced by the increased activity of glycolysis-regulatory enzymes hexokinase (HK; Fig. 2E), phosphofructokinase (PFK; Fig. 2F), and pyruvate kinase (PK; Fig. 2G) in tumors in the HFHS-fed mice as compared to those in Chow or CR groups. Further, we evaluated lactate dehydrogenase (LDH) activity (Fig. 2H) and quantified intratumoral lactate levels, which revealed an increase as a function of caloric intake (Fig. 2I). A similar pattern was observed in serum lactate levels in tumor-bearing mice but not in control groups, thereby indicating that tumors are responsible for the differences described above (Fig. S2a). Hepatic lactate levels were also evaluated and revealed that mice in both the CR and HFHS groups had lower lactate levels as compared to mice in the Chow group, which was not affected by the growing tumor (Fig. S2b). We also analyzed the conversion of pyruvate to lactate by LDH and the expression of the two LDH isoforms (*Ldha* and *Ldhb*) in the tumors. Our results indicate that there are no differences in the activity or expression of LDH induced by diet (Fig. S2c–e). Finally, the expression of unbalanced energy metabolism markers *Pthlh* and *Igfbp3*, both related to the wasting of tissues, were evaluated and revealed an upregulation of both genes in tumors from the HFHS group (Fig. 2J and K, respectively), which might be related to WAT wasting, as observed in Fig. 1. To further understand the effects of the diets on tumor metabolism, we treated B16F10 cells with serum from animals fed CR, Chow, and HFHS diets and evaluated the expression of genes related to lipid metabolism and the expression of *Pthlh* and *Igfbp3*. Our *in vitro* results were similar to those observed *in vivo* (Fig. S2f). In addition, we have treated HuH7 hepatoma cells and 3T3-L1 adipocytes with 200 μ M PA in high glucose medium. The conditioned medium (CM) from these cells was used to treat B16F10 cells. The expression of *Fabp3*, *Cd36*, and *Cpt1a* in B16F10 cells was slightly modulated by the presence of PA in the CM of HuH7 or 3T3-L1, or by PA supplementation in the culture medium of B16F10 cells (Fig. S2g–i). However, the expression of *Ppara*, *Pthlh*, and *Igfbp3* were upregulated by CM of 3T3-L1 incubated with 25 mM glucose and 200 μ M PA (Fig. S2j–l). These data together indicate that the energy metabolism in tumors in HFHS-fed mice is, in fact, exacerbated, which putatively contributes to the greater tumor growth in this group.

The tumorigenic process modulates the physiology and metabolism of liver tissue

Since the different diet regimens have consequences for tumor growth and metabolism, we evaluated the hepatic effects of both on liver metabolism and physiology. Figure 3A indicates a greater accumulation of TG in the liver of mice in the HFHS group, which is not altered by the growth of ectopic tumors in these animals. These data are corroborated by histologically evaluating the steatotic process in the HFHS group, which is slightly less evident in tumor-bearing HFHS mice (Fig. 3B, C). Moreover, cholesterol levels are increased in the livers of the HFHS group, which was not observed in the tumor-bearing mice (Fig. 3D). We also evaluated liver damage by measuring plasma levels of the enzymes AST and ALT, which are increased in HFHS controls as compared to Chow group (Fig. 3E, F, respectively). Curiously, in tumor-bearing HFHS animals, these markers of liver damage are reduced when compared to their control counterparts (Fig. 3E, F). Although, picosirius red staining does not indicate the

Fig. 1 | HFHS diet enhances body weight gain, glucose intolerance, and tumor growth which, in turn, induces weight loss in the HFHS group and glucose intolerance in the Chow group.

A Schematic of the protocol. Female mice (12-weeks-old) were fed a Chow diet *ad libitum* (Chow), caloric restriction (CR), or HFHS diet *ad libitum* for 23 weeks. An ectopic tumor was induced with B16F10 cells injection and after three additional weeks, mice were submitted to euthanasia as described in the “Materials and Methods” section. B Delta body weight (BW) between Day 0 and the 26th week. C Carcass weight without tumor mass. D Tumor weight. E Tumor volume. F Liver. G Inguinal white adipose tissue (iWAT). H gonadal WAT (gWAT) relative weight. I oGTT curves for the three control groups, CR, Chow, and HFHS. J oGTT curves for the three tumor-bearing groups, CR, Chow, and HFHS. K Fasting glycemia before euthanasia. L Area under the curve represented in (I). M Area under the curve represented in (J). N Plasma insulin levels. Each test was performed with at least nine animals ($n = 9-20$) and plotted values are mean \pm S.E.M. * $P < 0.05$; ** $P < 0.01$; *** $P < 0.001$; **** $P < 0.0001$. For panels B, C, F–H, K, and N, a two-way ANOVA was performed, followed by Tukey’s post-test. For panels D, E, L, and M, a one-way ANOVA was performed, followed by Tukey’s post-test.



establishment of liver fibrotic process in any group (Fig. 3G), the reticulin staining (Fig. 3H) shows a reduction in reticular fibers staining in the HFHS groups when compared with animals from the CR and Chow groups (Fig. 3H, I) suggesting the initiation of fibrotic disease. Furthermore, *Vim* and *Tgfb* mRNA expression are upregulated in the control HFHS group as compared to Chow (Fig. 3K, L, respectively). In general, the presence of a

growing tumor exacerbates the expression of these fibrosis markers - in addition to *Mmp9* (Fig. 3M) and *Krt18* (Fig. 3N)—in CR and Chow mice, while it does not affect their expression in the HFHS group, where expressions are, in general, upregulated by the diet and tumor growth does not present an additive effect (Fig. 3K–N, hatched vs green). Additionally, *Il6* mRNA expression is upregulated in CR as compared to Chow or HFHS

Table 1 | Effects of diet and tumor growth on serum lipid parameters in mice

	CR	CR tumor-bearing	Chow	Chow tumor-bearing	HFHS	HFHS tumor-bearing
Total triglycerides	0.48 ± 0.09	0.28 ± 0.03 ^a	0.39 ± 0.05	0.79 ± 0.12 ^b	0.69 ± 0.03 ^a	0.92 ± 0.11 ^{c,d}
Total CHOL	0.64 ± 0.04	0.52 ± 0.03	0.61 ± 0.03	0.75 ± 0.05 ^{b,c}	0.87 ± 0.03 ^a	0.96 ± 0.07 ^{c,e}
Total HDL	0.21 ± 0.03	0.20 ± 0.02	0.15 ± 0.02	0.20 ± 0.02	0.28 ± 0.02 ^b	0.21 ± 0.02 ^a
Total LDL	6.78 ± 0.60	8.07 ± 0.38 ^a	7.88 ± 0.45	11.01 ± 1.27 ^b	8.36 ± 0.86 ^{a,b}	23.11 ± 2.63 ^{c,d,e}

Serum lipid profile in all tumor-free or tumor-bearing mice from CR, Chow, and HFHS groups. Serum parameters are in $\mu\text{g}/\mu\text{L}$. All plotted values are mean \pm S.E.M. of four to five animals. For statistics, two-way ANOVA followed by Tukey's post-test was used and $P < 0.05$ was considered statistically significant.

Serum parameters are in $\mu\text{g}/\mu\text{L}$. Data are presented as means \pm SEM ($n = 4-5$).

CHOL cholesterol, LDL low-density lipoprotein, HDL high-density lipoprotein.

^aSignificantly different compared to CR.

^bSignificantly different compared to Chow.

^cSignificantly different compared to CR tumor-bearing.

^dSignificantly different compared to HFHS.

^eSignificantly different compared to Chow tumor-bearing.

control groups (Fig. 3J). Curiously, particularly in the CR group but to a lesser extent in the Chow group too, *Il6* expression is upregulated in tumor-bearing animals as compared to controls (Fig. 3J). Finally, we evaluated senescence markers, p21, p16, and TERT (Fig. 3O–Q), and SIRT1, phosphorylated p53 and pRB, as well as, proliferating cell nuclear antigen (PCNA) expression by immunoblotting (Figs. 3R and S3b–e), which supported that diet impacts the cellular senescence process according to the caloric intake (CR < Chow < HFHS). Nevertheless, the growing tumor substantially increases the expression of p21 and p16 in all experimental groups (Fig. 3O, P, black vs hatched bars) whereas we observed a negative correlation between TERT expression and tumor size (Figs. 3Q and 1D, E).

Further, we investigate hepatic metabolism to evaluate the insulin signaling pathway. For this, half of the animals in all groups were challenged by intraperitoneal administration of insulin (2 IU/kg) 15 min before euthanasia. The main proteins of the insulin signaling pathway were evaluated by immunoblotting of mice liver homogenates (Fig. 4A; densitometric analyses of the Western blots are plotted in S4). We evaluated the expression of the β -subunit of insulin receptor (IR β), where we observed a reduction in its expression in all tumor-bearing mice, regardless of the diet regimen (Figs. 4A and S4a). Analyzing the AKT phosphorylation at Thr308 and Ser473 residues, we show that all groups respond to the hormone by increasing their insulin-stimulated phosphorylation (Figs. 4A, S4b, c). The presence of tumors does not induce a modulation of the AKT (Thr308) phosphorylation level (Figs. 4A and S4b, hatched vs black bars, saline groups). However, we observed a significant reduction in AKT (Ser473) phosphorylation in tumor-bearing mice in the HFHS group (Figs. 4A and S4c, pink bars) compared to their tumor-free counterparts. Next, we assessed mTOR phosphorylation and its downstream effector, p70S6K. In the CR and Chow groups, tumor-bearing mice showed increased levels of mTOR phosphorylation as compared to their controls (Figs. 4A and S4d). However, in the HFHS group, tumor-bearing mice had lower basal phosphorylation levels of mTOR as compared to the control mice and were not as responsive to insulin as the other tumor-bearing groups—Chow and CR (Figs. 4A and S4d). Indeed, mTOR downstream effector phosphorylation revealed that the HFHS control group is insulin-resistant, which is aggravated by tumor growth (Figs. 4A and S4e for p-p70S6K/p70S6K). Therefore, we assessed whether insulin signaling could be compromised by an increase in PKC phosphorylation levels. In fact, our data indicates that PKC is more phosphorylated at Thr514 in tumor-bearing mice than in their non-tumor counterparts (Figs. 4B and S4f). Moreover, HFHS treatment stimulated this phosphorylation in basal and insulin-stimulated mice, but maintained the additional effect promoted by tumor growth (Figs. 4B and S4f). Overall, these data indicate that tumor growth induces a reduction in IR β expression as well as an increase in pPKC (Thr514), which compromises insulin signaling in the liver, particularly in the HFHS group. This is concurrent with other studies that report a pronounced sex difference in sensitivity to Western-like diets, with male mice becoming more obese, insulin resistant, and tolerant to impaired glucose

than female mice^{31–34}. Thus, our data support that tumor growth induces insulin resistance even in female mice.

We next analyzed lipid metabolism in the liver through immunoblotting (Fig. 4C; densitometric analyses of the Western blots are plotted in S4). Our results revealed a significant increase in ACLY phosphorylation (Ser455) induced by insulin in all groups (Figs. 4C and S4g). The presence of tumors was found to trigger increased phosphorylation of ACLY in CR mice but induce a reduction in pACLY (Ser455) levels in the Chow and HFHS groups (Figs. 4C and S4g). The inactive form of ACC—that is, pACC (Ser79)—did not respond to insulin stimulation in both control and tumor-bearing groups. Indeed, we observed increased phosphorylation in all HFHS groups as compared to their Chow counterparts (Figs. 4C and S4h). Moreover, there was a reduction in the expression of ACC in the HFHS group as compared to the Chow group (Figs. 4C and S4i), thereby indicating that this enzyme is inhibited in the liver of HFHS mice. Finally, we evaluated the expression of SCD1, an important marker of lipid metabolism. Our results revealed that SCD1 expression is not modulated by diet or insulin stimulation in control groups (Figs. 4C and S4j, hatched and gray bars). However, in tumor-bearing mice from all groups, this enzyme was found to be less expressed compared to their control counterparts (Figs. 4C and S4j). Furthermore, we analyzed the gene expression of proteins involved in lipid metabolism by qPCR. In the CR group, *Scd1* mRNA was upregulated as compared to the Chow group, and in tumor-bearing mice, *Scd1* was upregulated as compared to the control group (Fig. 4D). Yet, the downregulation of SCD1 reported in Fig. 4C is confirmed by qPCR for the HFHS group as compared to the Chow or CR groups (Fig. 4D). Conversely, we observed an increase in *Fgf21* expression in mice from the HFHS group, mainly in the tumor-bearing HFHS (Fig. 4E). Furthermore, our results indicated an increase in lipogenesis in the hepatocytes induced by the presence of tumors, as evidenced by the increased expression of the transcriptional factor *Xbp1s* (Fig. 4F) and upregulation of *APOB*, thereby suggesting increased triglyceride exportation by the liver (Fig. 4G). Moreover, we evaluated fatty acid mobilization and oxidation through the expression of *Cd36*, *Pgc1a*, *Cpt1a*, and *Acacl* (Fig. 4H, K, respectively). The overall results suggest that these genes are more expressed in the CR group in which a positive modulation by tumor growth is observed. Tumor growth also upregulated fatty acid mobilization and oxidation genes in Chow mice, thereby indicating the higher demand for energy in the liver upon the tumor growth process. In the HFHS group, our data suggest a reduction in fatty acid oxidation.

Tumor growth reduces the systemic inflammatory process

Given the importance of the inflammatory process for nonalcoholic fatty liver disease and insulin resistance, we evaluated the expression of the markers and mediators of this process. We began by evaluating the Kupffer cell population in the liver by analyzing the expression of *F4/80*, where we observed that the HFHS diet promotes a significant increase in Kupffer cells compared to the Chow diet, which is not modulated by tumor growth

(Fig. 5A). Further, we observed a decrease in TLR4 expression levels due to the caloric intake in both control and tumor-bearing animals (Fig. 5B, C). This expression pattern was also observed for pIKK (Fig. 5B, D) and iNOS

(Fig. 5B, E), thereby indicating an attenuated inflammatory profile in HFHS mice as compared to Chow mice. Curiously, tumor growth downregulated the inflammatory markers in all dietetic regimens (Fig. 5B, E).

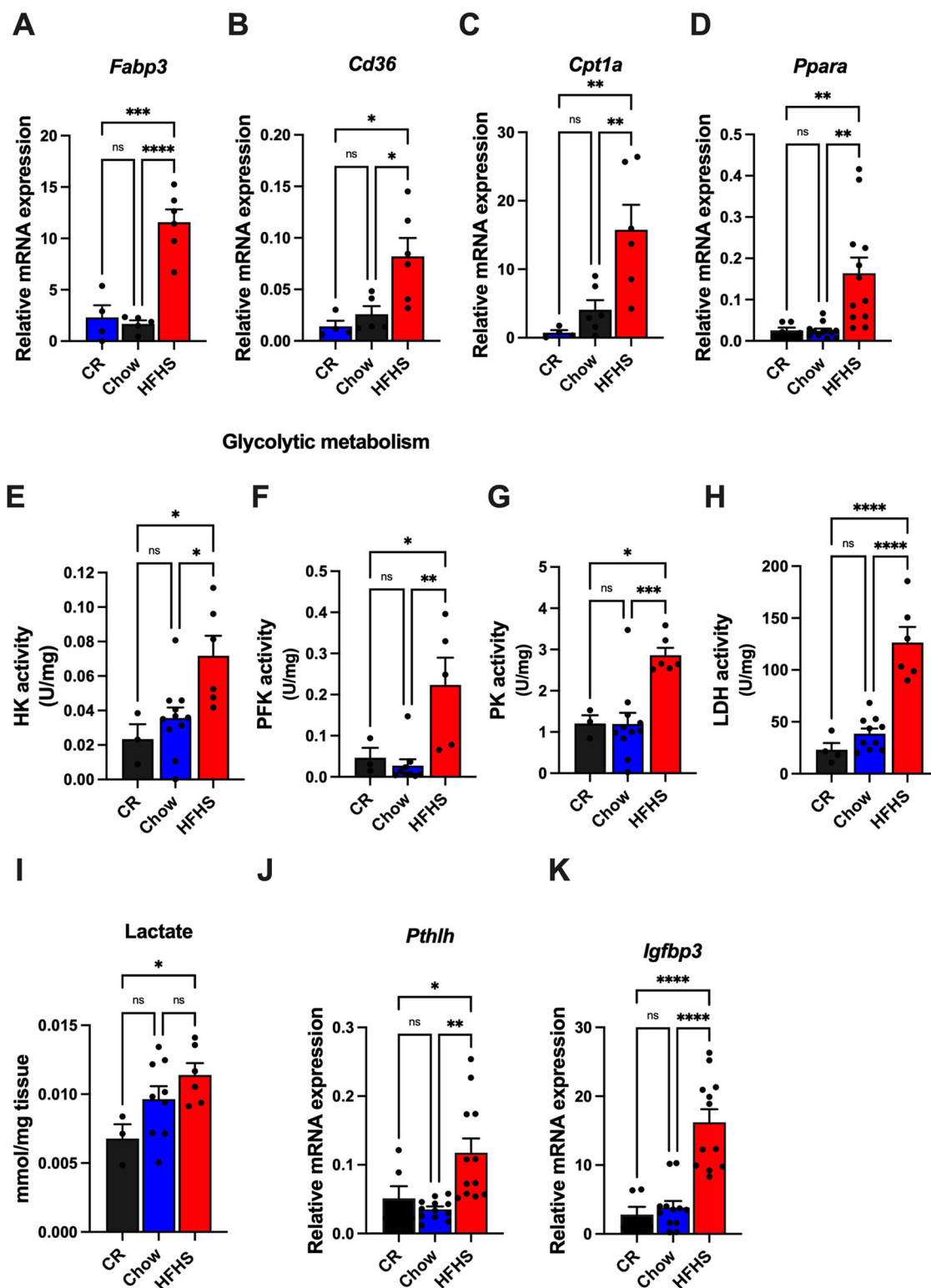
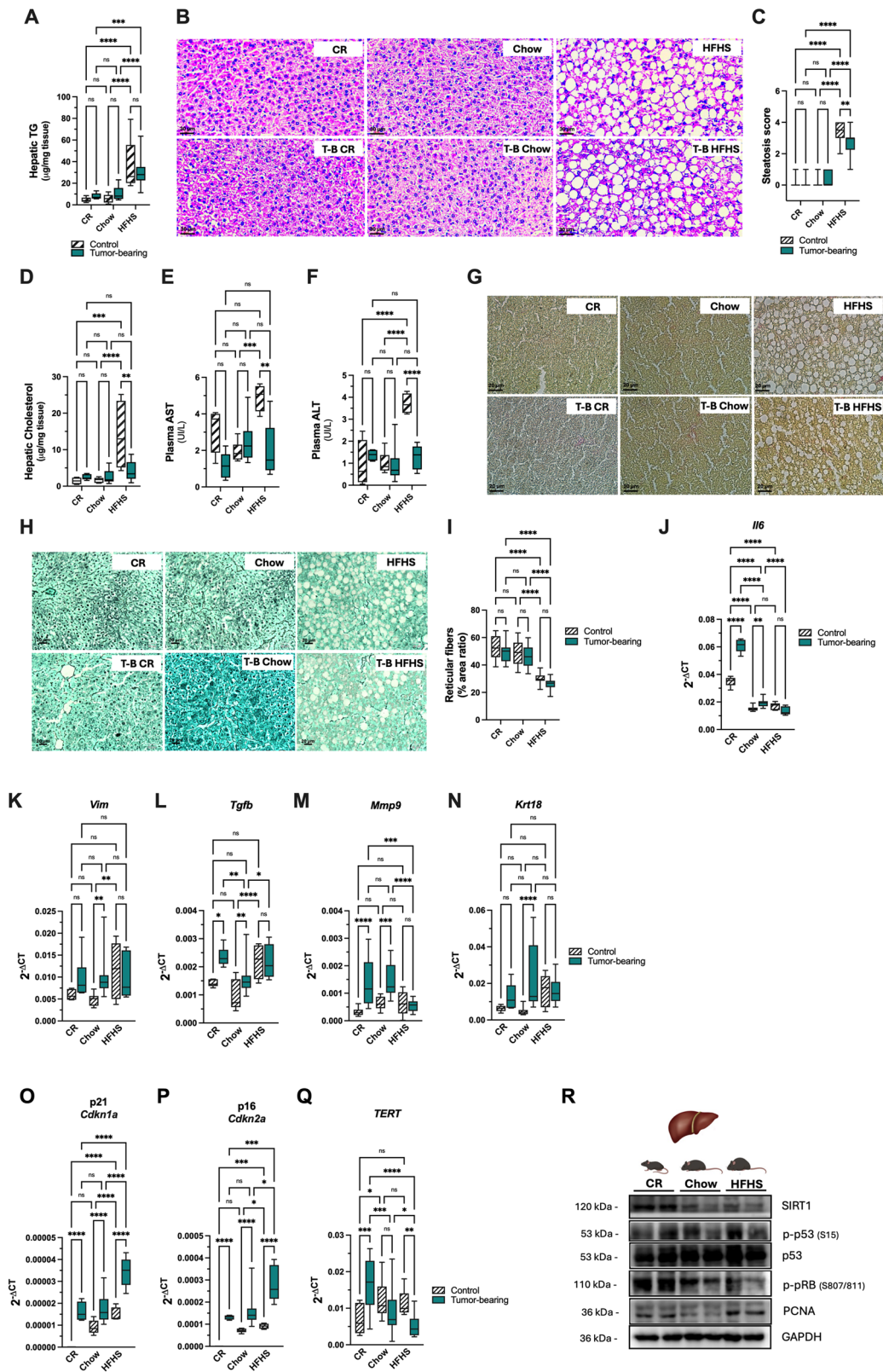


Fig. 2 | HFHS improves lipid and glucose metabolism in tumors and increases the expression of disruptors of energy balance. A Fatty acid binding protein 3 (*Fabp3*) expression. **B** Cluster of differentiation 36 (*Cd36*) mRNA expression. **C** Expression of carnitine palmitoyltransferase 1A (*Cpt1a*). **D** Expression of peroxisome proliferator-activated receptor alpha (*Ppara*). **E–G** Tumor glycolytic metabolism evaluated by hexokinase (HK) activity (E), phosphofructokinase (PFK) activity (F),

and pyruvate kinase (PK) activity (G). **H** Lactate dehydrogenase (LDH) activity. **I** Intratumor lactate levels. **J** Expression of parathyroid hormone-like hormone (*Pthlh*). **K** Expression of insulin-like growth factor binding protein 3 (*Igfbp3*). **P* < 0.05; ***P* < 0.01; ****P* < 0.001; *****P* < 0.0001. For all panels, a one-way ANOVA was performed, followed by Tukey’s post-test.



Additionally, we analyzed the inflammatory process in gWAT. Figure 5F depicts macrophage infiltration into gWAT and confirms that, such as in the liver, *F4/80* mRNA expression increased in the HFHS mice compared to that in the tumor-free Chow or CR mice. Interestingly, the tumorigenic process reduced macrophage infiltration in the gWAT across all groups (Fig. 5F, hatched vs black bars). Furthermore, the *Tnfa*

mRNA expression was reduced in Chow and HFHS mice compared to that in the CR group, which is not modulated by the tumor growth process (Fig. 5G). Figure 5H presents a representative immunoblotting, where a reduction in the expression of TLR4 (Fig. 5H, I) and iNOS (Fig. 5H, J) as a function of increasing caloric intake (CR > Chow > HFHS) is evident, which is not modulated by the tumor growth.

Fig. 3 | HFHS diet and tumor growth induce liver senescence, steatosis, and fibrosis. **A** Liver triglycerides levels. **B** Histopathology of liver steatosis. Representative liver sections from CR, Chow, and HFHS tumor-free (control) and tumor-bearing mice (T-B mice) were stained with hematoxylin and eosin (scale bar = 30 μ M). **C** Steatosis score. **D** Liver cholesterol levels. **E, F** AST and ALT liver enzyme levels. **G** Collagen staining with Picrosirius red stain. Scale bar = 20 μ M. **H** Silver impregnation to detect reticulin fibers. Scale bar = 20 μ M. **I** Reticular fibers quantification. **J** Interleukin 6 (*Il6*) mRNA expression. **K–N** Liver fibrosis markers evaluated by qPCR. **K** Vimentin (*Vim*), **L** Transforming growth factor beta (*Tgfb*), **M** Matrix metalloproteinase-9 (*Mmp9*), and **N** Keratin 18 (*Krt18*). **O–Q** Senescence

markers: p21 (*Cdkn1a*) (**O**), p16 (*Cdkn2a*) (**P**) and Telomerase reverse transcriptase (TERT) (**Q**) mRNA expression. **R** Representatives immunoblot analysis of Sirtuin 1 (SIRT1) expression, phosphorylated p53 (S15) and total p53 expression, phosphorylated Retinoblastoma protein (pRB) (S807/811) expression, and Proliferating cell nuclear antigen (PCNA) expression. GAPDH was used as a loading control. The results represent three independent experiments ($n = 3$). Western blot densitometries are in S3. Each test was performed with at least nine animals ($n = 9–20$) and plotted values are mean \pm S.E.M. * $P < 0.05$; ** $P < 0.01$; *** $P < 0.001$; **** $P < 0.0001$. For all panels, a two-way ANOVA was performed, followed by Tukey's post-test.

Moreover, TNF α expression was reduced in the HFHS group when compared to the Chow group (Fig. 5H, K), thereby reproducing in gWAT the reduced inflammatory profile observed in the liver. In general, these results indicate that the tumor growth process has a rather limited influence on the systemic inflammatory process, with the main determined by the type of diet consumed.

Tumor growth modulates adipose tissue metabolism

With the aim of clarifying the molecular mechanisms involved in the crosstalk between adipose tissue and the tumor, we evaluated lipogenesis, the browning process, and the insulin signaling pathway in gWAT. As previously described, adipose tissues are the tissues that had their weight reduced during the 15 days in which the tumor growth process developed in HFHS animals (Fig. 1G, H). This can be correlated with the increased PGC1 α expression in tumor-bearing mice as compared to their control counterparts in the HFHS group (Figs. 6A and S5a). Indeed, PGC1 α expression decreases as the energy intake increases (CR > Chow > HFHS; Figs. 6A and S5a). In the control groups, PPAR γ expression was not affected by caloric intake, although in tumor-bearing mice PPAR γ decreased as the caloric intake increased (CR > Chow > HFHS). Yet, its expression was increased in the CR and inhibited in HFHS tumor-bearing mice compared to diet-matched controls (Figs. 6A and S5b). Assessing ACLy and ACC expression, our results indicated a profound reduction in their expression in HFHS mice compared to the other groups (Figs. 6A, S5d, f). ACLy and ACC phosphorylation follows the same pattern seen for total proteins; however, when we evaluated pACLy (Ser455)/ACLy and pACC (Ser79)/ACC, our results reveal an increase in the phosphorylation of these enzymes in the HFHS compared to Chow mice (Figs. 6A, S5c, e), without modifications induced by tumor growth. Nevertheless, the expression of other lipogenic enzymes—such as SCD1 (Figs. 6A and S5g), *Fasn* (Fig. 6B), and ATGL (Fig. 6C)—followed a similar pattern and, thus, revealed a reduction in their expression in accordance with the caloric intake. Additionally, the down-regulation of *Fasn* mRNA expression was strongly intensified by tumor growth (Fig. 6B). Reduction in SCD1 expression is normally associated with an increase in adiponectin expression, as confirmed by evaluating *Adipoq* mRNA expression in gWAT (Fig. 6D). Furthermore, *Prdm16* and *Ucp1* expression - both WAT browning markers—were upregulated in HFHS mice as compared to the other dietetic regimens (Fig. 6E, F). This is particularly clear when we look at the prominent increase in *Ucp1* expression in tumor-bearing HFHS mice (Fig. 6F, hatched vs brown bars), the relevance of which is exacerbated by the overexpression of PGC1 α in this same group (Figs. 6A and S5a).

Finally, we evaluated the response to insulin stimulation in gWAT. Although there were no significant differences in the expression of IR β among all groups (Figs. 6G and S5h), PI3K phosphorylation (Tyr508) was significantly reduced in tumor-bearing mice compared to their tumor-free peers in each feeding regimen (Figs. 6G and S5i). Furthermore, insulin responsiveness was observed when we evaluated the phosphorylation of the downstream effectors of the insulin pathway, pAKT (Thr308) and pAKT (Ser473), pmTOR (Ser2448), and p-p70S6K (Thr421/Ser424). In general, we observed that the diet promoted a decrease in insulin signaling in accordance with the caloric intake (CR > Chow > HFHS), while the tumor growth process rescues the responsiveness to insulin in gWAT

(Figs. 6G and S5j–m). Overall, we can infer that tumor growth reverts insulin resistance in gWAT triggered by increased caloric intake.

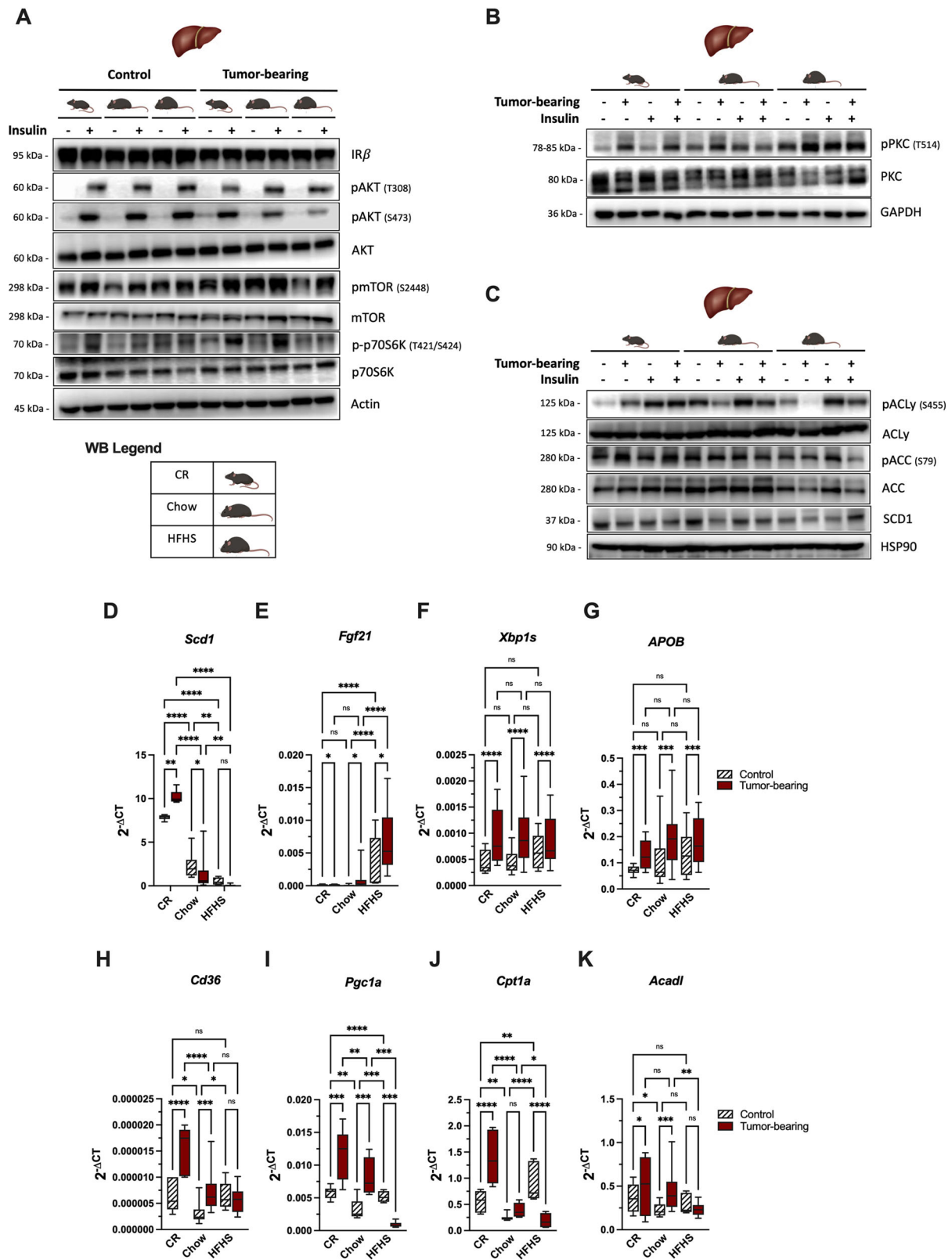
In an integrated manner, our data enable us to propose a model of crosstalk between tumors and liver and adipose tissues based on the results obtained in female mice fed the HFHS diet, which is presented in Fig. 6H.

Discussion

The daily lives and habits of humans change over the years as a result of different lifespan stages and ages. In this study, we investigated the metabolic consequences induced by changing the dietary regimen of young adult mice (after 12 weeks of age) and their impact on tumor growth. The findings of this study have to be seen in light of some limitations. The first is that we have used only female C57BL/6J mice, an underrepresented group due to the inequality of data regarding biological responses in females³⁵. In this context, current data indicate that the prevalence of obesity and severe obesity is higher in women than in men^{36,37} which reinforces the relevance of studying the effects of a hypercaloric diet in females. Furthermore, previous data indicate that, for most applications, female mice, across multiple rodent species and traits, tested through their hormonal cycle display no more variation than males do, although biological responses may vary between genders^{38–41}. Thus, generalizability is subsequently impacted regarding sex-based differences. The second limitation concerns the melanoma, a sexually dimorphic cancer⁴⁰. However, the current study used B16F10 cells because it is a model previously used in our studies in immunocompetent animals^{12,15}. In vivo, intradermal implant of B16F10 cells in C57BL/6 mice results in aggressively growing tumors showing efficient growth kinetics following a range of inoculation with a doubling time of approximately 2–3 days. In our previous studies, tumor growth of B16F10 cells was similar in males and females^{12,15}. Our goal here was to investigate the physiological responses induced by different dietary regimens on the senescence process and, consequently, on the biology of tissues, such as WAT and liver, during tumor growth.

We have previously shown and ratified here, that a “westernized” HFHS diet can accelerate the senescence process in animals subjected to this dietary regimen (Fig. 3S–U, and ref. 12), but this is not so for the ectopic tumors that are grown in these animals¹². A counterpoint to HFHS diet-induced aging could be achieved through caloric restriction, as demonstrated in several studies^{42–46}. Therefore, we also evaluated this dietary regimen in our model, where we showed that the tumor growth process prevents the benefits promoted by CR, for example, increasing the expression of senescence markers p21 and p16 (Fig. 3S, T), among others (Figs. 3U and S3a–e), in the liver. This effect of the tumor on the senescence process occurs despite the lower growth of tumor mass observed in CR mice compared to that in HFHS and Chow groups. Moreover, apart from the entire body, diet also feeds the tumor, as tumor weight and volume were found to increase as a function of increasing caloric input (CR > Chow > HFHS), as well as modulating tumor metabolism (Fig. S2f–l).

Indeed, tumors extracted from HFHS mice were found to have increased markers of uptake and oxidation of fatty acids, supporting the accelerated growth of these tumors and also explaining the reduction in WAT weight in these animals. In this context, adipose tissue is associated with metabolic syndromes and functions as an endocrine organ secreting cytokine, growth factors, and free fatty acids (FA), thereby supporting



tumorigenesis and metastasis⁴⁷. The uptake of free circulating FAs by tumors by FABP4 and CD36 promotes the activation of AMPK and, consequently, the increase in β -oxidation due to the greater expression of carnitine palmitoyltransferase 1 (CPT1 α) and acyl-CoA oxidase 1^{48,49}. In fact, higher CD36 expression is associated with a worse prognosis in different types of cancer^{2,50}. According to these authors, CD36 plays a key role in the

metabolic crosstalk between tumors and the microenvironment, inducing an exogenous lipids uptake on tumors to sustain the rapid proliferative rate of these cells⁵⁰. Our data indicated that the expression of CD36 and CPT1 α are exacerbated in the tumors of HFHS-fed mice, when compared to the other groups. Indeed, the increased uptake and oxidation of FAs by tumors and the increase in PPAR α activation were accompanied by the induction of

Fig. 4 | Tumor and diet-induced hepatic insulin resistance, impaired lipid metabolism, and liver-WAT crosstalk. To evaluate the insulin signaling pathway, a proportion of the animals received an insulin shot before euthanasia as described in the Materials and Methods section. **A** Representative immunoblot analysis of insulin receptor β (IR β) expression, phosphorylated AKT (T308 and S473), mTOR (S2448), and Ribosomal protein S6 kinase beta-1 (p70S6K) (T421/S424) expression. The total proteins or β -actin were used as loading control. **B** Representative immunoblotting of phosphorylated PKC (Thr514) and total PKC in liver lysates (GAPDH was used as loading control). **C** Representative immunoblotting of phosphorylated ATP citrate lyase (ACLY) (S455), acetyl-CoA carboxylase (ACC) (S79), and total ACLY, ACC, and stearyl-CoA desaturase 1 (SCD1) in liver lysates

(HSP90 was used as loading control). The results represent three independent experiments ($n = 3$). Western blot densitometries are in S4. **D** *Scd1*. **E** Fibroblast growth factor 21 (*Fgf21*). **F** Spliced form of X-box binding protein 1 (*Xbp1s*). **G** *ApoB* mRNA expression. **H** *Cd36*. **I** Peroxisome proliferator-activated receptor gamma coactivator 1-alpha (*Pgc1a*). **J** *Cpt1a* and **K** Acyl-CoA dehydrogenase long chain (*Acadl*) mRNA expression in liver from CR, Chow, or HFHS fed animals from all groups. Plotted values are mean \pm S.E.M. * $P < 0.05$; ** $P < 0.01$; *** $P < 0.001$; **** $P < 0.0001$. For all panels, a two-way ANOVA was performed, followed by Tukey's post-test. qPCR reactions for each sample were performed in duplicate. All liver samples were analyzed.

the epithelial-mesenchymal-transition (EMT), which is consistent with the increased incidence of metastasis^{2,12}. Furthermore, our data indicated wasting and browning of gWAT underway in these animals, which may have been induced by the overexpression of tumor-derived parathyroid-hormone-related protein (*Pthlh*) and insulin-growth factor binding protein (*Igfbp3*) in tumors, thereby demonstrating the crosstalk between these tissues. IGFBP was also increased in tumor tissues, which disrupts both insulin and IGF-1 signaling and operates as an inducer of cachexia as a multiorgan syndrome⁵¹. In turn, PTHrP plays an important role in the wasting of gWAT by driving the expression of thermogenic genes in adipose tissue⁵². Furthermore, the increased *Pthlh* expression observed in tumors from HFHS mice (Fig. 2J) may be due to an increase in tumor metabolic acidosis^{52,53}, since we observed a gradual increase in intratumoral lactate levels according to caloric intake, which is reflected in the serum levels of this marker. Moreover, there is an interorgan futile cycle, such as the Cori cycle, which can be activated between the liver and the tumor⁵⁴. This cycle plays an important role in compensating for tumor-induced acidosis, which occurs due to the use of tumor-derived lactate for gluconeogenesis. Indeed, circulating lactate levels were higher in HFHS tumor-bearing mice, while its levels were lower in the livers of these mice compared to Chow mice. On the other hand, glycemia in this group was increased, thereby indicating that lactate can serve as a gluconeogenic substrate. Furthermore, the reduction in lactate levels in the liver of HFHS-fed mice may be associated with a reduction in fatty acid synthesis⁵⁵; this reduction was even more pronounced in HFHS tumor-bearing mice. In fact, we showed here that there is a lower lipids synthesis in the liver and WAT with an increase in the caloric intake provided by the diet; this is further enhanced by the tumor growth (Figs. 4C and 6A).

Dyslipidemias are common conditions associated with fat-rich diets and are strong risk factors for other conditions such as atherosclerosis, cardiovascular diseases, type 2 diabetes, and cancer⁵⁶. Our data here indicate a different point of view on this correlation since the growing tumor, per se, induced a dyslipidemic profile and aggravated HFHS diet-induced dyslipidemia. This statement is based on a series of results as follows. The serum levels of triglycerides, LDL, and cholesterol are augmented in tumor-bearing HFHS-fed animals as compared to Chow or control HFHS-fed animals (Table 1) supporting the dyslipidemic profile. Moreover, serum metabolic analysis revealed the upregulation of phospholipid derivatives and lipid-modified amino acids in the tumor-bearing HFHS-fed group, suggesting an enhanced lipoprotein metabolism by this group (Fig. S6). Particularly, this last result combined with the high serum triglycerides is indicative of elevated VLDL production and released by the livers of these animals or increased VLDL metabolism via lipoprotein lipase by other tissues. This effect seems to be specific for phospholipids since other metabolites related to fatty acids synthesis and degradation are not significantly modified in the liver (Fig. S4k–n) nor in WAT (Fig. S5n–q). Indeed, the liver lipid profile indicates that increased VLDL production is a result of the HFHS diet since the effects of the diet are not modified in the liver by the growing tumor (Fig. S4o–r), but in WAT (Fig. S5r–u). Moreover, high lipoprotein lipase activity is a characteristic of cancers due to the increased need for phospholipids to support cellular division and growth⁵⁷.

Stearyl CoA desaturase 1 (SCD1) is a critical lipogenic enzyme and its reduced expression is associated with several other physiological functions,

including protection against diet-induced adiposity, hepatic steatosis, and hyperglycemia⁵⁸. Additionally, the inhibition of SCD1 promotes increased liver expression and elevated plasma levels of the fibroblast growth factor 21 (FGF21). Our data are in accordance with the literature and indicated an additional effect of the tumor growth process—increasing the expression of *Scd1* only in tumor-bearing CR mice and a reduction in its expression in accordance with the caloric intake. Therefore, we observed an increase in *Fgf21* expression, particularly in HFHS tumor-bearing mice. Further, the hepatokine FGF21 has a protective effect against diet-induced obesity, increases insulin sensitivity, stimulates lipolysis in adipose tissue, and decreases triglyceride levels in diabetic rodents⁵⁹. Here, the upregulation of *Fgf21* in HFHS tumor-bearing mice (Fig. 4E) correlated with lower fasting insulinemia, with no impact on fasting glycemia (Fig. 1N), a strong indicator of improvement of WAT insulin sensitivity of these mice. However, this increase in systemic insulin sensitivity induced by FGF21 was not observed in the liver⁶⁰, thereby confirming the results observed in this study (Figs. 4A and S4). Furthermore, XBP1s, the FGF21 transcriptional factor, is usually upregulated in liver tissues of NASH patients and is known to increase lipogenesis in hepatocytes⁶¹. In this study, XBP1s levels increased in response to the tumorigenic process in mice from all groups compared to their tumor-free counterparts (Fig. 4F). Further, *APOB* upregulation is related to an increase in TG export, while the expression of *Cd36* is associated with the uptake of FAs. *Cd36* is a fatty acid translocase that directly contributes to the development of fatty liver under conditions of high free FA modulating the rate of FA uptake by hepatocytes⁶². Here, serum parameters for TG and LDL were found to be compatible with the *ApoB* expression in the liver (Table 1 and Fig. 4G). The elevated cholesterol levels in the serum of HFHS mice and, mainly, HFHS tumor-bearing mice observed in this study are in line with data from the literature that reveal that serum CHOL levels are associated with an increased incidence and recurrence of several types of cancer^{50,63}. Furthermore, the increase in *ApoB* expression—with reduced hepatic cholesterol content observed in HFHS tumor-bearing mice (Fig. 3D)—indicated that the export of lipoproteins is favored in these mice.

The induction of cachexia due to increased energy expenditure and the activation of tumor-triggered thermogenesis led to the browning of WAT^{64,65}. As confirmed here, the levels of UCP1, a hallmark of the adipocyte browning process, are dramatically upregulated in the tumor-bearing HFHS group, the same group where WAT wasting was observed. In addition to UCP1, tumors also induce the expression of other browning markers, such as *Prdm16* and *Adipoq*. The latter is directly associated with the effect of FGF21 on adipose tissue^{60,66}.

Furthermore, we observed a downregulation of genes associated with FA oxidation (*Pgc1a*, *Cpt1a*, and *Acadl*) in the livers of tumor-bearing mice according to the caloric intake provided to these animals. Moreover, *PGC1a*, in addition to being a negative regulator of hepatic FGF21 expression⁵⁹, promotes an increased expression of enzymes involved in gluconeogenesis and FA oxidation, among other actions^{67,68}. In mice, the decrease in *PGC1a* expression induces steatosis and hepatic insulin resistance in animals subjected to HFD^{68,69}. However, this condition increases whole-body insulin sensitivity and glucose tolerance, partially due to FGF21 upregulation. In fact, our data reveal that insulin signaling was compromised in the liver of HFHS tumor-bearing mice but not in the gWAT of these animals, where it

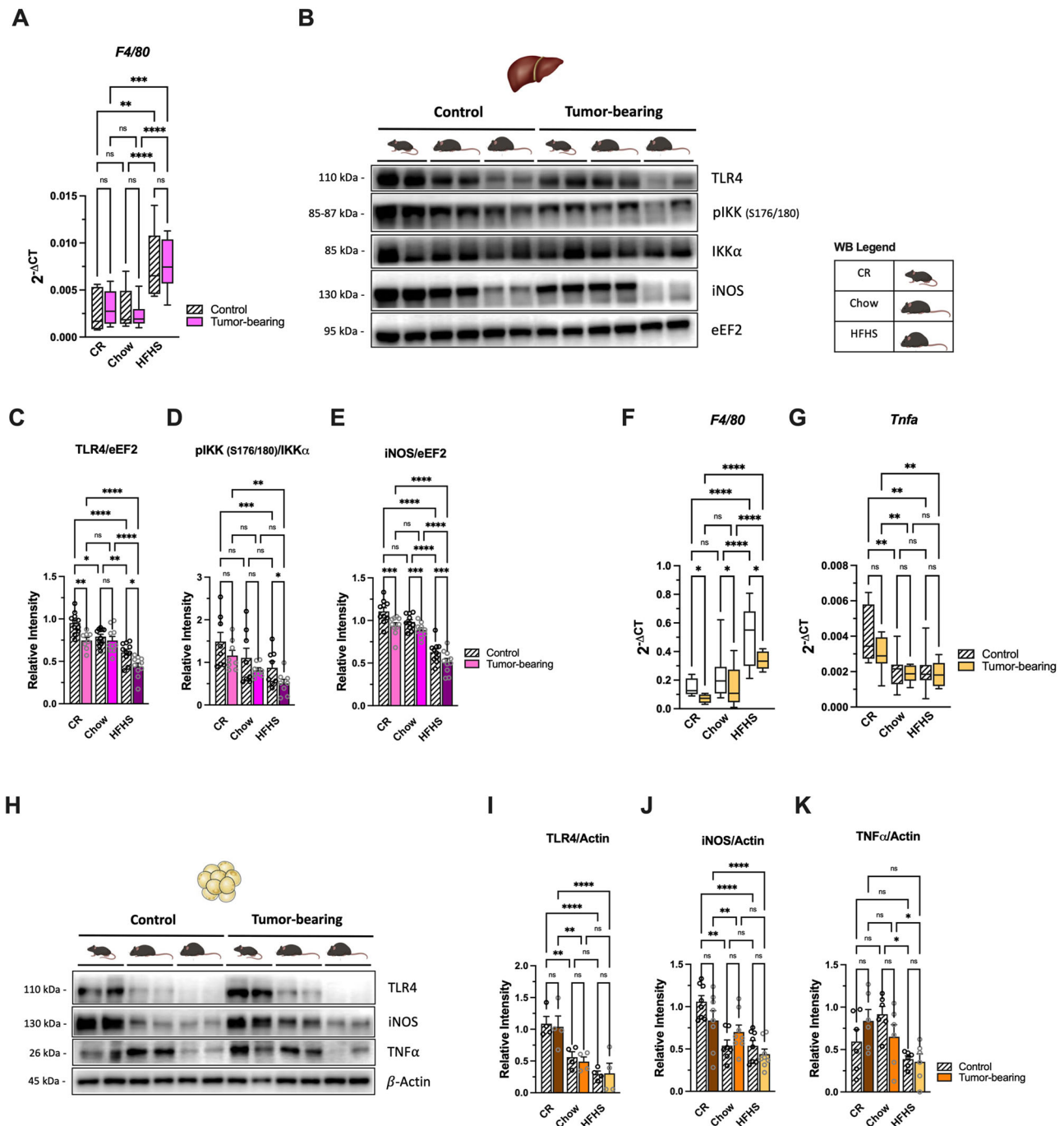
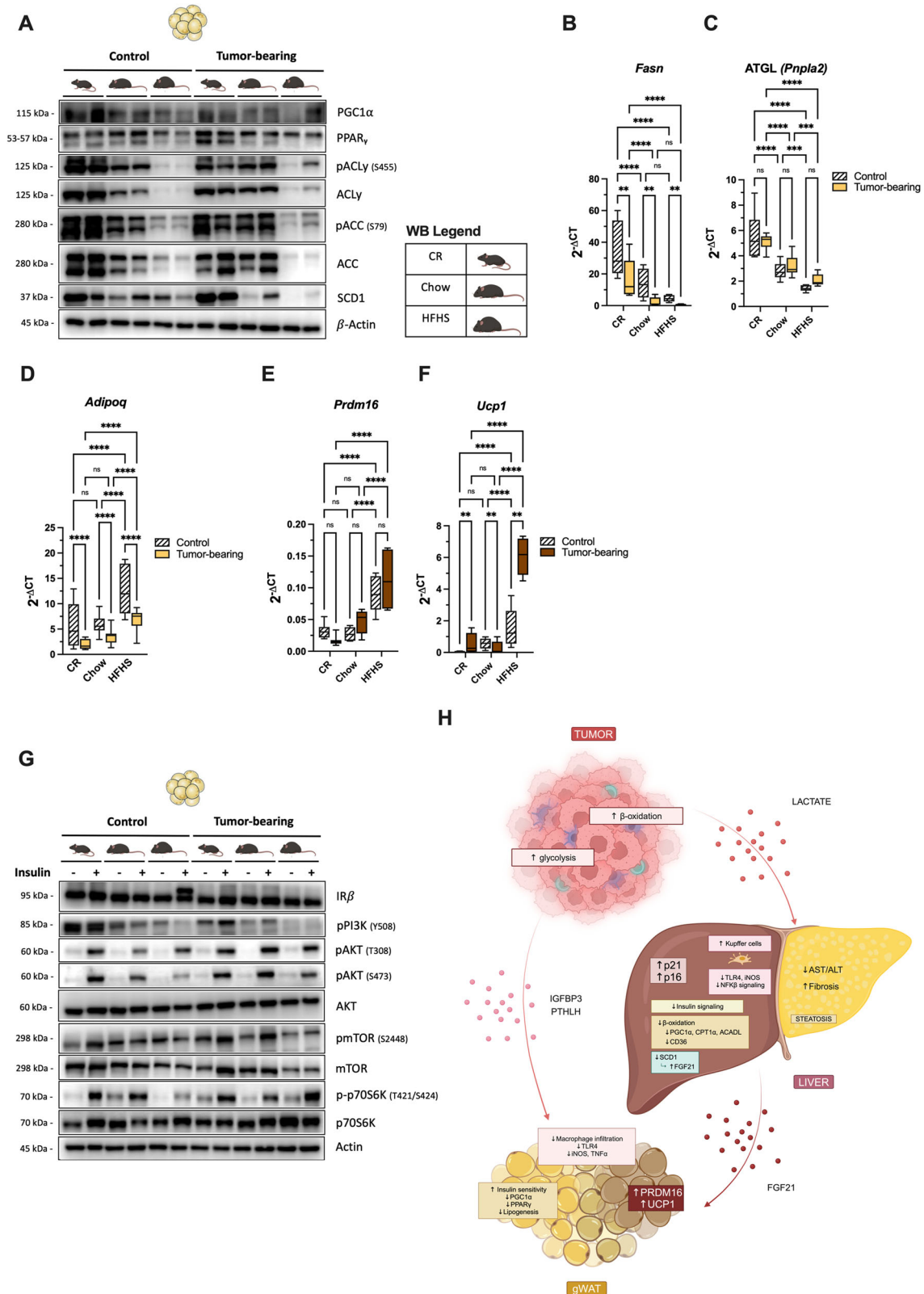


Fig. 5 | Liver and gWAT inflammation are downregulated by dietary caloric input and tumor growth. **A** qPCR analysis of liver Kupffer cells/macrophage population: *F4/80* expression. Immunoregulation in liver lysates was evaluated by Western blot in control (tumor-free) and tumor-bearing samples from CR, Chow, or HFHS-fed mice. **B** Representative immunoblotting of Toll-like receptor 4 (TLR4), phosphorylated I κ B kinase (IKK) (S176/180), IKK α , and inducible nitric oxide synthase (iNOS) in liver samples. eEF2 was used as a loading control. (C–E) Western blotting densitometry quantifications of **C** TLR4/eEF2, **D** pIKK (S176/180)/IKK α , and **E** iNOS/eEF2. The results are from three independent experiments ($n = 3$). **F**, **G** qPCR analysis of gWAT macrophage infiltration, **F** *F4/80*, and **G** *Tnfa*

expression. Immunoregulation in gWAT lysates was evaluated by Western blot in control (tumor-free) and tumor-bearing samples from CR, Chow, or HFHS-fed mice. **H** Representative immunoblotting of TLR4, iNOS, and TNF α protein expression in gWAT lysates. β -actin was used as a loading control. **I–K** Western blotting densitometry quantifications of **I** TLR4/Actin, **J** iNOS/ β -actin, and **K** TNF α / β -actin. The results represent three independent experiments ($n = 3$). Plotted values are mean \pm S.E.M. * $P < 0.05$; ** $P < 0.01$; *** $P < 0.001$; **** $P < 0.0001$. For all panels, a two-way ANOVA was performed, followed by Tukey’s post-test. qPCR reactions for each sample were conducted in duplicate and all tissue samples were analyzed.

was partially reestablished. This is particularly evident when we evaluate the phosphorylation of pAKT (S473) and p-p70S6K (T421/S424) in gWAT. Furthermore, the reduction in hepatic SCD1 expression leads to the upregulation of GLUT4 and adiponectin in adipose tissue⁵⁸, thus favoring insulin signaling.

Increased adiposity impacts tumorigenesis, as the excess of nutrients and increased levels of pro-inflammatory cytokines act as drivers of tumorigenesis in different types of cancer^{70–72}. Inflammatory and insulin responses are regulated by TLR4 expression⁷³. In this study, we showed that, in both liver and gWAT, the increase in caloric intake was associated with a



reduction in TLR4 expression (Fig. 5B, C, as well as H, I). Moreover, growing tumors potentiated TLR4 downregulation in these animals as well. Therefore, the systemic inflammatory response in these animals was disrupted. These results may be due to several factors. For example, hyperinsulinemia—which occurs concomitantly with obesity—downregulates TLR4 expression⁷⁴. Furthermore, aging—which is accelerated by an HFHS diet¹²—also induces

a decrease in TLR4 expression⁷⁵. Nevertheless, we also need to consider that here we evaluated all these processes in female mice, in which estrogen levels can modulate TLR4 expression⁷⁶ and aromatase levels are altered in parallel with the increase in adiposity^{77,78}. Furthermore, TLR4 is differentially modulated by saturated and unsaturated fatty acids^{79,80}. Our HFHS diet had approximately 30% saturated fat and 70% unsaturated fat, with mainly oleic

Fig. 6 | Tumor growth induces browning and reverts insulin resistance in WAT from HFHS-fed mice. Lipid metabolism regulation in gWAT lysates was evaluated by western blot in control (tumor-free) and tumor-bearing samples from CR, Chow, or HFHS-fed mice. **A** Representative immunoblotting of PGC1 α , PPAR γ , phosphorylated ACLy (S455) and ACC (S79), and ACLy, ACC, and SCD1 protein expressions in gWAT lysates. Actin was used as a loading control. **B–D** qPCR analysis of **B** fatty acid synthase (*Fasn*), **C** adipose triglyceride lipase (ATGL, *Pnpla2*), and **D** Adiponectin (*Adipoq*) expression. **E, F** Browning markers expressions: **E** PR/SET domain 16 (*Prdm16*) and **F** uncoupling protein 1 (*Ucp1*) mRNA expression. To evaluate the insulin signaling pathway, a proportion of the animals

received an insulin shot before euthanasia, as described in the Materials and Methods section. **G** Representative immunoblot analysis of insulin receptor β (IR β) expression, phosphorylated PI3K (Y508), AKT (T308 and S473), mTOR (S2448), and p70S6K (T421/S424) in gWAT lysates. Total proteins or β -actin were used as loading control. Western blot densitometries are in S6. **H** Model of crosstalk between tumor-liver-WAT in HFHS mice. Created in BioRender. Xavier do Nascimento Júnior, J. (2024) BioRender.com/e43f529. Plotted values are mean \pm S.E.M. * $P < 0.05$; ** $P < 0.01$; *** $P < 0.001$; **** $P < 0.0001$. For all panels, a two-way ANOVA was performed, followed by Tukey's post-test. qPCR reactions for each sample were conducted in duplicate and all tissue samples were analyzed.

and linoleic acids. Therefore, the impairment of inflammation observed here may be an adaptive response of these female mice to various disruptors of the immune process.

Our previous studies indicate that high-caloric diets rich in refined sugars and excess fat can disrupt metabolic homeostasis^{36,81,82}. In this study, an HFHS diet promoted hepatic steatosis, which is not affected by the tumor growth process in tumor-bearing mice. The fatty liver disturbed Picrosirius red staining⁸³, yet HFHS tumor-free mice presented elevated AST and ALT levels as compared to the mice in the other two groups. These enzymes, in addition to being indicators of liver damage, are also indirect markers of initial-phase liver fibrosis, which was supported by lower levels of reticular fibers in mice in the HFHS group as compared to those in the CR or Chow groups (Figs. 3E, F, as well as H, I). However, we observed a reduction in serum AST and ALT levels in HFHS tumor-bearing mice compared to their control counterparts. Nonetheless, reticular fibers, Keratin 18, Vimentin, and TGF β were upregulated in the HFHS group livers and their expression was triggered by the tumorigenic process in the other groups. TGF- β can induce EMT, and fibrogenesis⁸⁴ and is associated with hepatocellular carcinoma (HCC)⁸⁵. Furthermore, IL-6 is a potent hepatocyte mitogen implicated in liver regeneration⁸⁶. These findings strongly suggest that there was a modulation of liver physiology in response to the presence of an ectopic tumor in these mice, which was higher in the HFHS group.

Finally, our results revealed the contribution of exacerbated caloric intake to metabolic syndrome and aging-related diseases in addition to its role in encouraging the incidence and progression of cancer. Nevertheless, further research on the molecular mechanisms underlying the observed metabolic and inflammatory alterations in aging and cancer will be necessary. Therefore, understanding the nutritional-based interventions' effects on dysbiosis, failing immunosurveillance, and gender responses to this age-associated metabolic syndrome is the current focus of our research.

Data availability

The data used to support the findings of this study are available in Supplemental Data 1 and 2. Uncropped blot/gels are available in Supplemental Material S8. Metabolomic raw data are available in the repository Dryad (<https://datadryad.org>)⁸⁷. All other data are available from the corresponding author upon reasonable request.

Received: 8 July 2024; Accepted: 31 December 2024;

Published online: 07 January 2025

References

- Calle, E. E. & Kaaks, R. Overweight, obesity and cancer: epidemiological evidence and proposed mechanisms. *Nat. Rev. Cancer* **4**, 579–591 (2004).
- Huang, J. et al. Adipocyte p62/SQSTM1 suppresses tumorigenesis through opposite regulations of metabolism in adipose tissue and tumor. *Cancer Cell* **33**, 770–784.e6 (2018).
- Wolin, K. Y., Carson, K. & Colditz, G. A. Obesity and cancer. *Oncologist* **15**, 556–565 (2010).
- López-Otín, C., Galluzzi, L., Freije, J. M. P., Madeo, F. & Kroemer, G. Metabolic control of longevity. *Cell* **166**, 802–821 (2016).
- Barzilai, N., Huffman, D. M., Muzumdar, R. H. & Bartke, A. The critical role of metabolic pathways in aging. *Diabetes* **61**, 1315–1322 (2012).
- Gorgoulis, V. et al. Cellular senescence: defining a path forward. *Cell* **179**, 813–827 (2019).
- Guo, J. et al. Aging and aging-related diseases: from molecular mechanisms to interventions and treatments. *Signal Transduct. Target Ther.* **7**, 391 (2022).
- Rodier, F. & Campisi, J. Four faces of cellular senescence. *J. Cell Biol.* **192**, 547–556 (2011).
- Paramos-de-Carvalho, D., Jacinto, A. & Saúde, L. The right time for senescence. *Elife* **10**, e72449 (2021).
- Efeyan, A., Comb, W. C. & Sabatini, D. M. Nutrient-sensing mechanisms and pathways. *Nature* **517**, 302–310 (2015).
- Lee, J. H., Budanov, A. V. & Karin, M. Sestrins orchestrate cellular metabolism to attenuate aging. *Cell Metab.* **18**, 792–801 (2013).
- Imbroisi Filho, R. et al. Western diet leads to aging-related tumorigenesis via activation of the inflammatory, UPR, and EMT pathways. *Cell Death Dis.* **12**, 643 (2021).
- Ogden, C. L., Yanovski, S. Z., Carroll, M. D. & Flegal, K. M. The epidemiology of obesity. *Gastroenterology* **132**, 2087–2102 (2007).
- Pfluger, P. T., Herranz, D., Velasco-Miguel, S., Serrano, M. & Tschö, M. H. Sirt1 protects against high-fat diet-induced metabolic damage. *PNAS* **105**, 9793–9798 (2008).
- Ochioni, A. C. et al. Clotrimazole presents anticancer properties against a mouse melanoma model acting as a PI3K inhibitor and inducing repolarization of tumor-associated macrophages. *Biochim. Biophys. Acta Mol. Basis Dis.* **1867**, 166263 (2021).
- Penforis, P. & Marette, A. Inducible nitric oxide synthase modulates lipolysis in adipocytes. *J. Lipid Res* **46**, 135–142 (2005).
- Charan, J. & Kantharia, N. How to calculate sample size in animal studies? *J. Pharm. Pharmacother.* **4**, 303–306 (2013).
- Anhê, F. F. et al. Treatment with camu camu (*Myrciaria dubia*) prevents obesity by altering the gut microbiota and increasing energy expenditure in diet-induced obese mice. *Gut* **68**, 453–464 (2019).
- Faustino-Rocha, A. et al. Estimation of rat mammary tumor volume using caliper and ultrasonography measurements. *Lab Anim.* **42**, 217–224 (2013).
- Branco, J. R. et al. Dietary citrate acutely induces insulin resistance and markers of liver inflammation in mice. *J. Nutr. Biochem.* **98**, 108834 (2021).
- Folch, J., Lees, M. & Sloane Stanley, G. H. A simple method for the isolation and purification of total lipides from animal tissues. *J. Biol. Chem.* **226**, 497–509 (1957).
- Ausina, P. et al. Acetylsalicylic acid and salicylic acid present anticancer properties against melanoma by promoting nitric oxide-dependent endoplasmic reticulum stress and apoptosis. *Sci. Rep.* **10**, 19617 (2020).
- Nascimento Júnior, J. X. D., Sola-Penna, M. & Zancan, P. Clotrimazole reverses macrophage M2 polarization by disrupting the PI3K/AKT/mTOR pathway. *Biochem. Biophys. Res. Commun.* **696**, 149455 (2024).
- Furtado, C. M., Marcondes, M. C., Sola-Penna, M., de Souza, M. L. S. & Zancan, P. Clotrimazole preferentially inhibits human breast cancer cell proliferation, viability and glycolysis. *PLoS One* **7**, e30462 (2012).
- Mota, L. A. M. et al. Culture of mouse peritoneal macrophages with mouse serum induces lipid bodies that associate with the

- parasitophorous vacuole and decrease their microbicidal capacity against *Toxoplasma gondii*. *Mem. Inst. Oswaldo Cruz* **109**, 767–774 (2014).
26. Demaria, T. M. et al. Once a week consumption of Western diet over twelve weeks promotes sustained insulin resistance and non-alcoholic fat liver disease in C57BL/6J mice. *Sci. Rep.* **13**, 3058 (2023).
 27. Fischer, A. H., Jacobson, K. A., Rose, J. & Zeller, R. Hematoxylin and eosin staining of tissue and cell sections. *Cold Spring Harb. Protoc.* **3**, pdb.prot4986 (2008).
 28. Junqueira, L. C. U., Bignolas, G. & Brentani, R. R. Picrosirius staining plus polarization microscopy, a specific method for collagen detection in tissue sections. *Histochem. J.* **11**, 447–455 (1979).
 29. Gömöri, G. Silver impregnation of reticulum in paraffin sections. **13**, 993–1002.5 (1937).
 30. Sola-Penna, M. et al. A radioassay for phosphofructokinase-1 activity in cell extracts and purified enzyme. *J. Biochem. Biophys. Methods* **50**, 129–140 (2002).
 31. Pettersson, U. S., Waldén, T. B., Carlsson, P. O., Jansson, L. & Phillipson, M. Female mice are protected against high-fat diet induced metabolic syndrome and increase the regulatory T cell population in adipose tissue. *PLoS One* **7**, e46057 (2012).
 32. Medrikova, D. et al. Sex differences during the course of diet-induced obesity in mice: adipose tissue expandability and glycemic control. *Int. J. Obes.* **36**, 262–272 (2012).
 33. Ingvorsen, C., Karp, N. A. & Lelliott, C. J. The role of sex and body weight on the metabolic effects of high-fat diet in C57BL/6N mice. *Nutr. Diabetes* **7**, e261 (2017).
 34. Daniels Gatward, L. F., Kennard, M. R., Smith, L. I. F. & King, A. J. F. The use of mice in diabetes research: the impact of physiological characteristics, choice of model and husbandry practices. *Diabet. Med.* **38**, e14711 (2021).
 35. Plevkova, J. et al. Various aspects of sex and gender bias in biomedical research. *Physiol. Res.* **69**, S367–S378 (2021).
 36. Hales, C. M., Carroll, M. D., Fryar, C. D. & Ogden, C. L. *Prevalence of Obesity and Severe Obesity Among Adults: United States, 2017–2018 Key Findings Data From the National Health and Nutrition Examination Survey* (NCHS, 2017).
 37. Cooper, A. J., Gupta, S. R., Moustafa, A. F. & Chao, A. M. Sex/gender differences in obesity prevalence, comorbidities, and treatment. *Curr. Obes. Rep.* **10**, 458–466 (2021).
 38. Beery, A. K. Inclusion of females does not increase variability in rodent research studies. *Curr. Opin. Behav. Sci.* **23**, 143–149 (2018).
 39. Vellera, H. L., Letsinger, A. C., Walker, N. R., Granados, J. Z. & Lightfoot, J. T. High fat high sugar diet reduces voluntary wheel running in mice independent of sex hormone involvement. *Front. Physiol.* **8**, 628 (2017).
 40. Chhabra, Y. et al. Sex-dependent effects in the aged melanoma tumor microenvironment influence invasion and resistance to targeted therapy. *Cell* **187**, 6016–6034.e25 (2024).
 41. Fish, E. N. The X-files in immunity: sex-based differences predispose immune responses. *Nat. Rev. Immunol.* **8**, 737–744 (2008).
 42. Piper, M. D. W., Partridge, L., Raubenheimer, D. & Simpson, S. J. Dietary restriction and aging: a unifying perspective. *Cell Metab.* **14**, 154–160 (2011).
 43. Madeo, F., Carmona-Gutierrez, D., Hofer, S. J. & Kroemer, G. Caloric restriction mimetics against age-associated disease: targets, mechanisms, and therapeutic potential. *Cell Metab.* **29**, 592–610 (2019).
 44. Longo, V. D. & Anderson, R. M. Nutrition, longevity and disease: From molecular mechanisms to interventions. *Cell* **185**, 1455–1470 (2022).
 45. Mihaylova, M. M. et al. When a calorie is not just a calorie: diet quality and timing as mediators of metabolism and healthy aging. *Cell Metab.* **35**, 1114–1131 (2023).
 46. Lim, G. M., Maharajan, N. & Cho, G. W. How calorie restriction slows aging: an epigenetic perspective. *J. Mol. Med.* **102**, 629–640 (2024).
 47. Nieman, K. M., Romero, I. L., Van Houten, B. & Lengyel, E. Adipose tissue and adipocytes support tumorigenesis and metastasis. *Biochim. Biophys. Acta Mol. Cell Biol. Lipids* **1831**, 1533–1541 (2013).
 48. Nieman, K. M. et al. Adipocytes promote ovarian cancer metastasis and provide energy for rapid tumor growth. *Nat. Med.* **17**, 1498–1503 (2011).
 49. Ladanyi, A. et al. Adipocyte-induced CD36 expression drives ovarian cancer progression and metastasis. *Oncogene* **37**, 2285–2301 (2018).
 50. Koundouros, N. & Pouligiannis, G. Reprogramming of fatty acid metabolism in cancer. *Br. J. Cancer* **122**, 4–22 (2020).
 51. Yeom, E. & Yu, K. Understanding the molecular basis of anorexia and tissue wasting in cancer cachexia. *Exp. Mol. Med.* **54**, 426–432 (2022).
 52. Kir, S. et al. Tumour-derived PTH-related protein triggers adipose tissue browning and cancer cachexia. *Nature* **513**, 100–104 (2014).
 53. Beck, N. & Webster, S. K. Effects of acute metabolic acidosis on parathyroid hormone action and calcium mobilization. *Am. J. Physiol.* **230**, 127–131 (1976).
 54. Argilés, J. M., Fontes-Oliveira, C. C., Toledo, M., López-Soriano, F. J. & Busquets, S. Cachexia: a problem of energetic inefficiency. *J. Cachexia Sarcopenia Muscle* **5**, 279–286 (2014).
 55. Li, X. et al. Lactate metabolism in human health and disease. *Signal Transduct. Target Ther.* **7**, 305 (2022).
 56. Zhang, Y.-Y. et al. Effects of T2DM on cancer progression: pivotal precipitating factors and underlying mechanisms. *Front. Endocrinol.* **15**, 1396022 (2024).
 57. Yan, Y. C. et al. Diacylglycerol lipase alpha promotes hepatocellular carcinoma progression and induces lenvatinib resistance by enhancing YAP activity. *Cell Death Dis.* **14**, 404 (2023).
 58. Aljohani, A. et al. Hepatic stearyl CoA desaturase 1 deficiency increases glucose uptake in adipose tissue partially through the PGC-1 α -FGF21 axis in mice. *J. Biol. Chem.* **294**, 19475–19485 (2019).
 59. Estall, J. L. et al. PGC-1 negatively regulates hepatic FGF21 expression by modulating the heme/Rev-Erb axis. *PNAS* **106**, 22510–22515 (2009).
 60. Lin, Z. et al. Adiponectin mediates the metabolic effects of FGF21 on glucose homeostasis and insulin sensitivity in mice. *Cell Metab.* **17**, 779–789 (2013).
 61. Wang, Q. et al. Role of XBP1 in regulating the progression of non-alcoholic steatohepatitis. *J. Hepatol.* **77**, 312–325 (2022).
 62. Wilson Camella, G. et al. Hepatocyte-specific disruption of CD36 attenuates fatty liver and improves insulin sensitivity in HFD-Fed mice. *Endocrinology* **157**, 570–585 (2016).
 63. Kuzu, O. F., Noory, M. A. & Robertson, G. P. The role of cholesterol in cancer. *Cancer Res.* **76**, 2063–2070 (2016).
 64. Petruzzelli, M. et al. A switch from white to brown fat increases energy expenditure in cancer-associated cachexia. *Cell Metab.* **20**, 433–447 (2014).
 65. Kir, S. & Spiegelman, B. M. Cachexia and brown fat: a burning issue in cancer. *Trends Cancer* **2**, 461–463 (2016).
 66. Machado, S. A. et al. Browning of the white adipose tissue regulation: new insights into nutritional and metabolic relevance in health and diseases. *Nutr. Metab.* **19**, 61 (2022).
 67. Matthew Morris, E. et al. Pgc-1 α overexpression results in increased hepatic fatty acid oxidation with reduced triacylglycerol accumulation and secretion. *Am. J. Physiol. Gastrointest. Liver Physiol.* **303**, G979–G992 (2012).
 68. Wan, X. et al. PGC1 α protects against hepatic steatosis and insulin resistance via enhancing IL10-mediated anti-inflammatory response. *FASEB J.* **34**, 10751–10761 (2020).
 69. Leone, T. C. et al. PGC-1 α deficiency causes multi-system energy metabolic derangements: muscle dysfunction, abnormal weight control and hepatic steatosis. *PLoS Biol.* **3**, 0672–0687 (2005).

70. De Marzo, A. M., Nakai, Y. & Nelson, W. G. Inflammation, atrophy, and prostate carcinogenesis. *Urol. Oncol.* **25**, 398–400 (2007).
71. Sutcliffe, S. & Platz, E. A. Inflammation in the etiology of prostate cancer: An epidemiologic perspective. *Urol. Oncol.* **25**, 242–249 (2007).
72. Ouchi, N., Parker, J. L., Lugus, J. J. & Walsh, K. Adipokines in inflammation and metabolic disease. *Nat. Rev. Immunol.* **11**, 85–97 (2011).
73. Jia, L. et al. Hepatocyte toll-like receptor 4 regulates obesity-induced inflammation and insulin resistance. *Nat. Commun.* **5**, 3878 (2014).
74. De Laat, M. A. et al. Hyperinsulinemia down-regulates TLR4 expression in the mammalian heart. *Front. Endocrinol.* **5**, 120 (2014).
75. Renshaw, M. et al. Cutting edge: impaired toll-like receptor expression and function in aging. *J. Immunol.* **169**, 4697–4701 (2002).
76. Meng, Q. et al. Activation of estrogen receptor α inhibits TLR4 signaling in macrophages and alleviates the instability of atherosclerotic plaques in the postmenopausal stage. *Int. Immunopharmacol.* **116**, 109825 (2023).
77. Mcternan, P. G. et al. Gender differences in the regulation of P450 aromatase expression and activity in human adipose tissue. *Int. J. Obes.* **24**, 875–881 (2000).
78. Wang, X., Simpson, E. R. & Brown, K. A. Aromatase overexpression in dysfunctional adipose tissue links obesity to postmenopausal breast cancer. *J. Steroid Biochem. Mol. Biol.* **153**, 35–44 (2015).
79. Lee, J. Y., Sohn, K. H., Rhee, S. H. & Hwang, D. Saturated fatty acids, but not unsaturated fatty acids, induce the expression of cyclooxygenase-2 mediated through toll-like receptor 4. *J. Biol. Chem.* **276**, 16683–16689 (2001).
80. Shi, H. et al. TLR4 links innate immunity and fatty acid-induced insulin resistance. *J. Clin. Investig.* **116**, 3015–3025 (2006).
81. Branco, J. R. et al. Citrate enrichment in a western diet reduces weight gain via browning of adipose tissues without resolving diet-induced insulin resistance in mice. *Food Funct.* **13**, 10947–10955 (2022).
82. Costa-Bartuli, E. et al. The role of interferon receptors α/β /yablation during western diet-induced obesity and insulin resistance in the inflectional model AG129 mice strain. *J. Interferon Cytokine Res.* **43**, 287–298 (2023).
83. Lattouf, R. et al. Picrosirius red staining: a useful tool to appraise collagen networks in normal and pathological tissues. *J. Histochem. Cytochem.* **62**, 751–758 (2014).
84. Dooley, S. & Ten Dijke, P. TGF- β in progression of liver disease. *Cell Tissue Res.* **347**, 245–256 (2012).
85. Bissell, D. M., Roulot, D. & George, J. Transforming growth factor β and the liver. *Hepatology* **34**, 859–867 (2001).
86. Streetz, K. L., Luedde, T., Manns, M. P. & Trautwein, C. Interleukin 6 and liver regeneration. *Gut* **47**, 309–312 (2000).
87. Zancan, Patricia. *Metabolomics Data for “Dietary Caloric Input and Tumor Growth Accelerate Senescence and Modulate Liver and Adipose Tissue Crosstalk”*. <https://doi.org/10.5061/dryad.d7wm37qb3> (DRYAD, 2024).
- 444675/2023-0; and Conselho Coordenação de Aperfeiçoamento de Pessoal de Nível Superior (CAPES).

Author contributions

J.X.d.N.J., J.d.C.G., A.B.A., and J.R.B. performed western blots and qPCR experiments. R.I.F., A.d.O.E.M., J.G.B.L., and T.M.D. ran the animal protocol and experiments. H.d.M.V. performed histological assays. L.D.C., A.C.O., and L.P.P. performed the extraction and quantification of lipids and lactate, respectively. J.X.d.N.J., M.S.-P., and P.Z. extensively discussed the results. P.Z. conceived the work and wrote the paper. J.X.d.N.J., M.S.-P., and P.Z. reviewed and edited the paper.

Competing interests

The authors declare no competing interests.

Ethical approval

The animal protocol was adhered to in accordance with the fundamental principles indicated by the International Council for Laboratory Animal Science (ICLAS) and the criteria approved by the Animal Care and Use Committee from the Health Sciences Center of the Federal University of Rio de Janeiro. The following is the approved protocol number: CEUA/CCS/UFRJ 177/18.

Additional information

Supplementary information The online version contains supplementary material available at <https://doi.org/10.1038/s42003-025-07451-y>.

Correspondence and requests for materials should be addressed to Patricia Zancan.

Peer review information *Communications Biology* thanks Lingdi Wang, and the other, anonymous, reviewers for their contribution to the peer review of this work. Primary Handling Editors: Soona Shin, Manuel Breuer, and Johannes Stortz. A peer review file is available.

Reprints and permissions information is available at <http://www.nature.com/reprints>

Publisher's note Springer Nature remains neutral with regard to jurisdictional claims in published maps and institutional affiliations.

Open Access This article is licensed under a Creative Commons Attribution-NonCommercial-NoDerivatives 4.0 International License, which permits any non-commercial use, sharing, distribution and reproduction in any medium or format, as long as you give appropriate credit to the original author(s) and the source, provide a link to the Creative Commons licence, and indicate if you modified the licensed material. You do not have permission under this licence to share adapted material derived from this article or parts of it. The images or other third party material in this article are included in the article's Creative Commons licence, unless indicated otherwise in a credit line to the material. If material is not included in the article's Creative Commons licence and your intended use is not permitted by statutory regulation or exceeds the permitted use, you will need to obtain permission directly from the copyright holder. To view a copy of this licence, visit <http://creativecommons.org/licenses/by-nc-nd/4.0/>.

© The Author(s) 2025

Acknowledgements

The authors thank Prof. Eduardo Cargnin-Ferreira (IFSC), Prof. Tatiana Maron Gutierrez, Prof. Andrea Da Poian (IBqM – UFRJ), and Lucas Ferreira dos Santos (IOC/FIOCRUZ), who kindly provided analytical tools. This work was supported by grants from Programa de Oncobiologia/Fundação do Câncer; Fundação de Amparo à Pesquisa do Estado do Rio de Janeiro (FAPERJ)—grants: E- 26/201.060/2022, E-26/210.651/2023, and E-26/210.065/2023; Conselho Nacional de Desenvolvimento Científico e Tecnológico (CNPq)—grant: 402918/2023-1, CNPq/DECIT (MS)—grant: